A MICROSCOPIC INVESTIGATION OF COCHLIOBOLOUS HETEROSTROPHOUS INFECTION IN MAIZE

by

Katharine Rita Minker

A thesis submitted to the Faculty of the University of Delaware in partial fulfillment of the requirements for the degree of Master of Science in Biological Sciences

Fall 2015

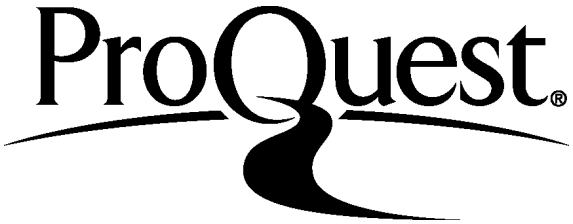

A MICROSCOPIC INVESTIGATION OF

COCHLIOBOLOUS HETEROSTROPHOUS INFECTION

IN MAIZE

by

Katharine Rita Minker

Approved: _____

Jeffrey L. Caplan, Ph.D.
Professor in charge of thesis on behalf of the Advisory Committee

Approved: _____

Robin W. Morgan, Ph.D.
Chair of the Department of Biological Sciences

Approved: _____

George H. Watson, Ph.D.
Dean of the College of Arts and Sciences

Approved: _____

Ann L. Ardis, Ph.D.
Interim Vice Provost for Graduate and Professional Education

ACKNOWLEDGMENTS

First, I would have not even applied to the graduate program if it weren't for the constant love of and inspiration of my Papa, Jack Minker. He has always advocated for educational achievement and who am I to disappoint? The presence of positive, caring mentors in my education is the reason I could write this thesis today. Antonio "Tango" Thomas was the first advisor to take a real interest in my success (and the first who can attest to my habitual last minute-ness). Karen Redden would then encourage my interests in plant genetics in college and introduce me to the research world. It was with their encouragement and recommendations that I would take the next step in my education.

My superhuman advisor Jeff Caplan has done so much for me. He and Randy Wisser gave me a project that maintained my interests the entire time. Both were extremely patient with me regardless of how many times I messed up. Jeff let me take time from lab to study for classes, he spoke to people on my behalf when my grades slipped, he helped me study for prelims, and prepare for talks. He always found me free food… Without Jeff's guidance and motivation I would not have made it this far. Thanks so much Jeff, I really hope the students that follow me in your lab are less dramatic.

TABLE OF CONTENTS

LIST OF FIGURES

ABSTRACT

Maize is an important crop with a number of uses ranging from valuable food source to biofuel. It is afflicted, like many other grasses, by a number of different pathogens. Southern Leaf Blight (SLB) is a disease that leads to significant crop loss and subsequent negative economic impact worldwide. A number of methods are in place to protect crops against this disease and other related pathogens however the most practical and sustainable form of defense is natural resistance. Quantitative disease resistance (QDR), conditioned by multiple quantitative trait loci (QTL), is a durable form of genetic protection conditioned by multiple genes that offer varying contributions to disease resistance. The mechanisms by which each QTL can enhance the level of resistance is largely unknown. A more in depth understanding of each QTL is necessary for maize breeders to grow maize lines of superior resistance, taste, and quality. In this project, I developed a fluorescence microscopy method to investigate pathogenesis in order to characterize the mechanisms of QDR at a cellular level. Combining advances in fluorescence confocal microscopy with a new clearing and staining technique, I was able to visualize and quantify plant fungal interactions in three dimensions (3D) during a time course of disease progression. I began the investigation by comparing two inbred lines of maize with extreme differences in susceptibility. B73 and Mo17 were ranked 258th and 22nd in resistance to SLB respectively based on robust phenotyping of 309 maize lines. Image analysis that detects and measures the amount of fungal infection and features of the infection networks identified quantifiable differences between the two lines. Furthermore, the study of fungal pathogenesis revealed a heterogeneity of fungal penetration and a distribution of invasion or colonization mainly along the vascular tissue. In the future,

these methods and features of pathogenesis will be used to examine nearly isogenic line (NIL) pairs contrasting for alleles at a single QTL to reveal clues about the mechanisms of genes for QDR.

Chapter 1

INTRODUCTION

Zea mays or maize is one of the highest yielding grains in the world. It is a valuable food source for humans and farm animals and can be converted into biofuels [1]. Maize, wheat, sorghum and other important grass crops are often afflicted by pests and pathogens that debilitate plant development. One such foliar pathogen is *Cochliobolous heterostrophous* which causes Southern Leaf Blight (SLB) on maize. SLB is an aggressive, necrotrophic, foliar disease. The most economical and sustainable form of defense is natural genetic resistance [23] which varies widely within maize.

Two understood categories of genetic resistance are used in plant disease studies, qualitative and quantitative. Quantitative disease resistance (QDR) is partial resistance conditioned by many genes and is considered far more durable than qualitative disease resistance [4]. In maize, some disease resistance genes have been identified as being heavily concentrated in certain chromosomal areas and are called quantitative trait loci (QTL) while others are may have genes spread across the genome. Some QTL may even only contain one gene that contributes to resistance however mapping resolution does not permit precision down to a single gene. Previous research on the individual effects of genes in QTL faced a number of challenges such as a repeatable way to quantify presence of pathogens in 3D [5].

In studies of disease resistance, most phenotyping is carried out on whole plants. While there are benefits to measuring whole plant variation, many of the

underlying cellular mechanisms of resistance go unnoticed. Microscopy can be used to measure unique features of pathogenesis that result in macroscopic effects. Establishing a protocol by which populations designed for genetic studies can be analyzed by high resolution microscopy is an essential step in the advancement of comparative biology [6].

In my project, I developed techniques specific for juvenile maize leaves infected with the fungal pathogen *C.heterostrophous* to be utilized in a semi-automated platform for collection of high resolution 3D image data that can be quantified and analyzed repeatedly without bias.

1.1 *Zea mays*

Maize is an important grain crop that has been cultivated for centuries. The plant originates from Central America and has been introduced to countries in Africa, North and South America, Asia, and Europe [1]. Its versatility has enabled the plant to adapt to a wide range of climactic environments. Breeders must consider a number of factors that contribute to plant development before selecting a variety of maize to cultivate. Such influences include; temperature, amount of daylight, soil-type, rain, and the intended purpose after harvest [1]. While most farmers grow maize for animal feed or the production of ethanol [1], those who grow for human consumption must also consider taste and cob quality.

The average development time for maize is around 110 days and is divided into five phases (Figure 1) [1]. Throughout the life cycle, leaves are among the most important plant organ. Leaves allow for the exchange of gasses and can carry out photosynthesis, producing its own nutrients. Maize is a typical monocot, its leaves demonstrate parallel venation connected by dispersed transverse vascular bundles all

of which are abnormally shaped. Cross sectional studies of maize leaves indicate that vascular bundles grow in three different sizes and can be characterized by the distinct number and type of cells that surround them (Figure 2) [7]. Small, intermediate, and large vascular bundles are all responsible for the conductivity of nutrients throughout a leaf.

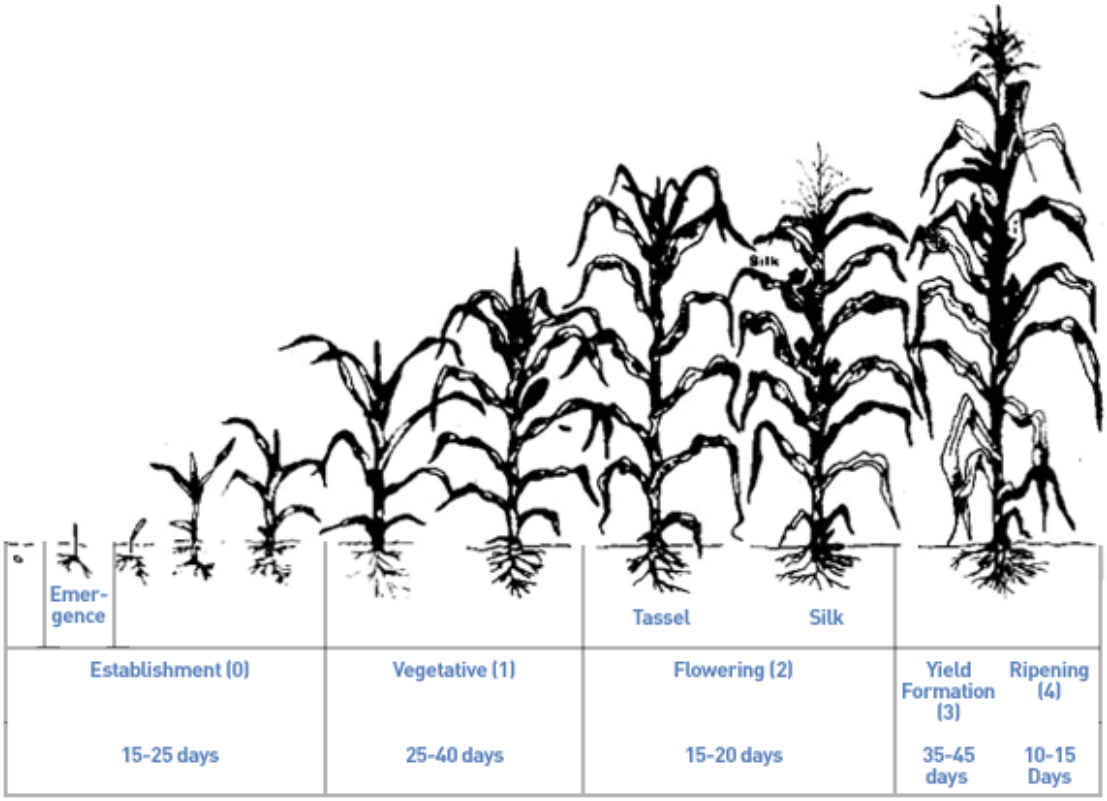

Figure 1 Schematic graph of maize growth (figure from Food and Agricultural Organization of the United Nations). Maize development is separated into different phases. The duration and name of each phase is shown.

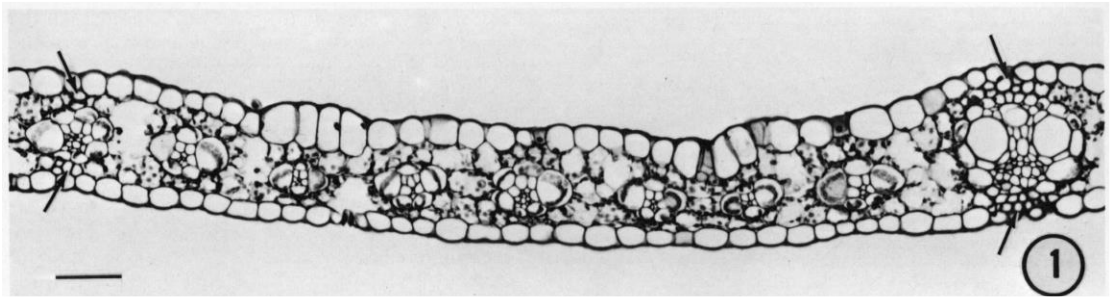

Figure 2 Maize leaf blade cross section (figure modified from Russell and Evert 1985). Arrows point to tightly packed sclerenchyma cells associated with large (far right) and intermediate (far left) vascular bundles. Cells surrounding the seven small bundles are arranged more loosely. Scale bar = 75 µm

Like all plants and animals, maize is afflicted by a number of diseases and pests. Foliar diseases in particular can be quite debilitating, as they interfere with the plants ability to provide itself with nutrients. Fungal pathogens create lesions on leaves that vary in size and intensity. Fungicides targeted for *C.heterostrophous* are obtainable but they can be costly and consumers are less interested in chemically treated foods. Natural disease resistance varies between different lines of maize, and lines with high level resistance can be used as a defense against disease [3].

Maize is used as a model organism for plant genetics. In 2002 the Maize Genome Sequencing Project was launched, and in 2009 the genome assembly of maize inbred line B73 was released. Since then numerous publications containing gene annotations, karyotypes, DNA methylation patterns, HapMap data, genome wide association studies (GWAS), and more have become available [8,9]. Understanding the influences of different genes is key to breeding a superior quality maize.

1.1.1 Maize Inbred Lines

Inbred lines are stocks of plants that have been crossed to a related plant in the same line. This results in offspring with the same genetic background as its parents. Two inbred lines can be crossed to create a hybrid that may be superior to its parent lines. Inbred lines are an especially important tool in genetic studies particularly in the development of quantitative trait locus mapping and linkage disequilibrium [10]. Maize has a very repetitive genome (Figure 3) separated into ten chromosomes. Its repetitiveness can make mapping and resequencing efforts very difficult. A strong familiarity of the historical and genetic relationship between related lines is needed, along with an understanding of how genetic diversity is partitioned in order to design experiments that will provide in depth analytical information.

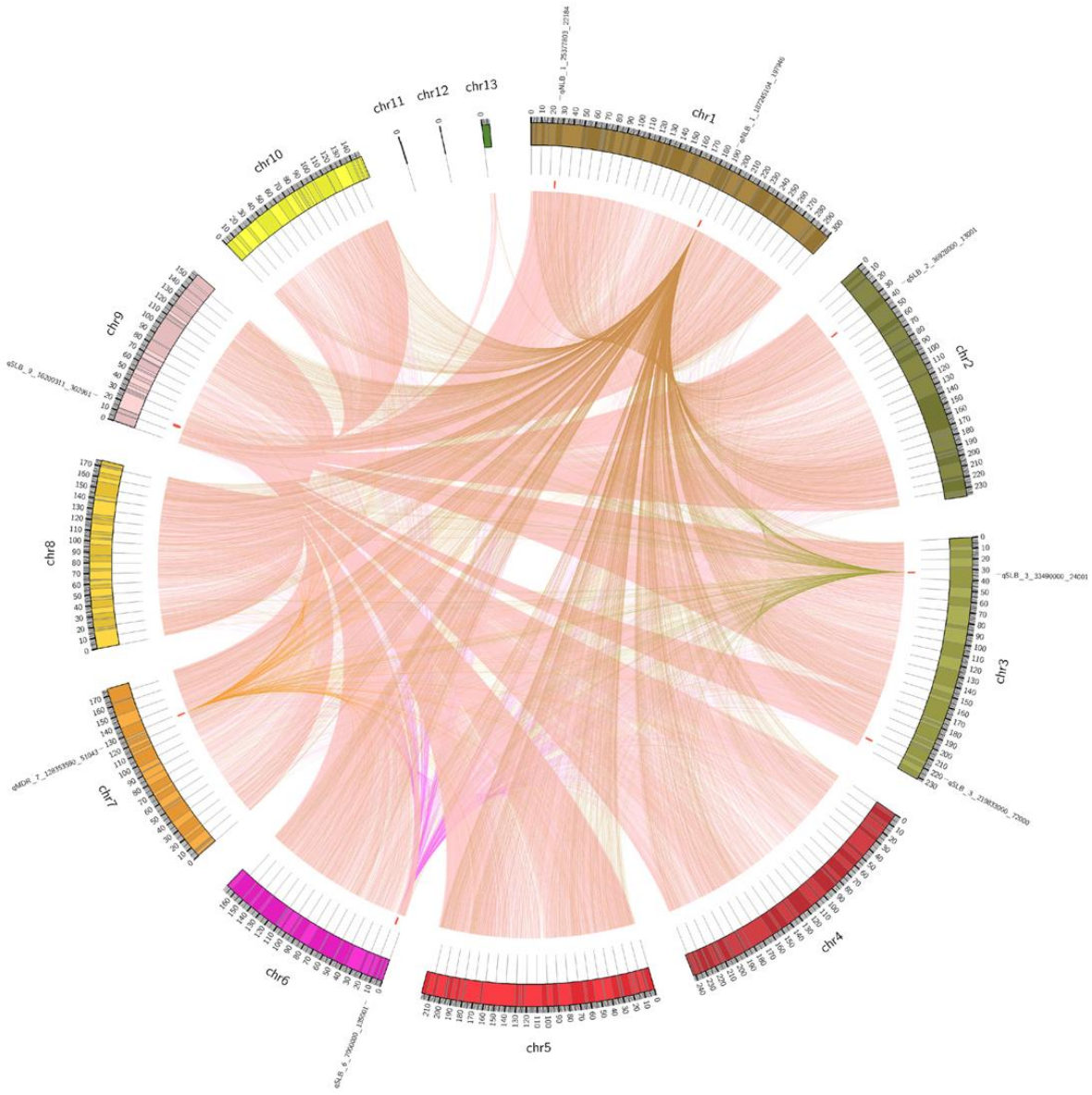

Figure 3 Repeats on maize genome greater than 5k base pairs. This map generated by PhD student Felix Francis shows where repetitive elements are found and on which chromosomes they also repeat.

1.1.2 Nested Association Mapping

A new design to interpret complicated traits in maize known as Nested Association Mapping (NAM) integrates linkage disequilibrium (LD) and association

mapping [11]. A population was designed using 25 founders that represent most genetic diversity worldwide. Each founder was crossed to B73 and self-fertilized to produce 25 segregating F_2 populations. From each population 200 recombinant inbred lines (RILs) were developed (Figure 4). This extensive set of RILs, nested within these 25 populations allow researchers to collaborate and contribute to community databases [11].

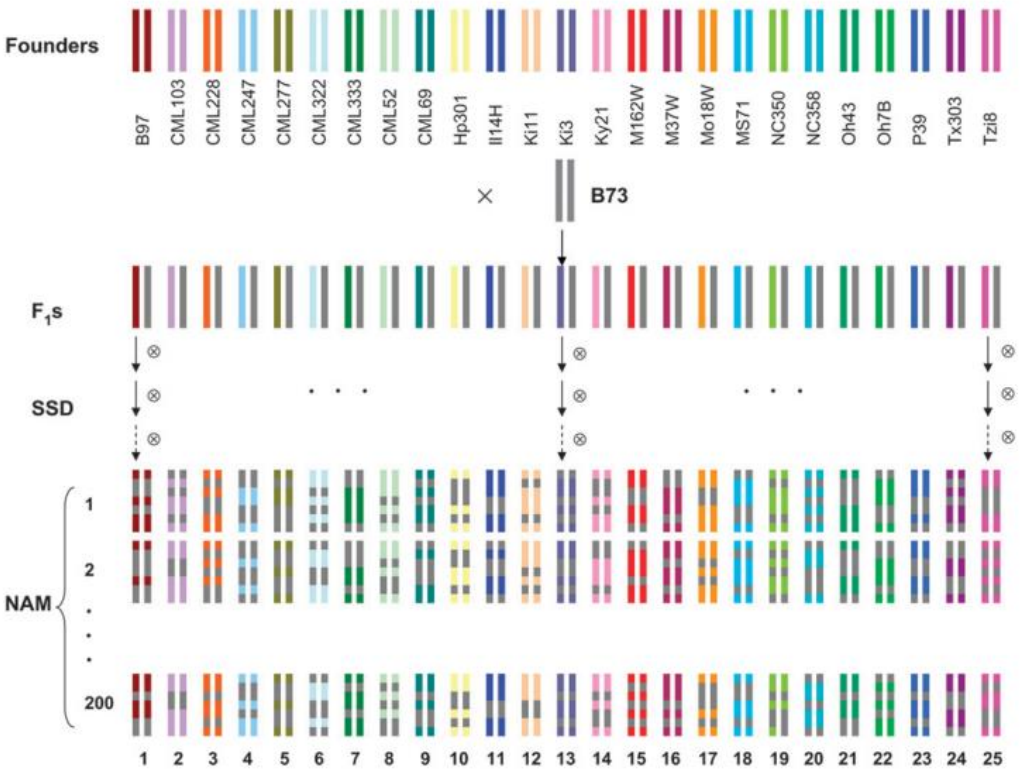

Figure 4 Nested Association Mapping populations (figure from Yu et al. 2008)

1.1.3 Qualitative vs Quantitative Disease Resistance

Disease resistance in maize is categorized in two general types. Qualitative disease resistance is strong resistance conferred by a single gene often called an R-

gene. While R-genes often have large effects [4], this type of resistance is usually race specific and is easily overcome by evolving pathogens[12]. In contrast quantitative disease resistance (QDR), is partial resistance conditioned by multiple genes of small effect. Collectively these genes form quantitative trait loci (QTL). Mapping R-genes can be done easily using Mendelian genetics, QTL are difficult to map because each gene has a modest phenotypic effect.

1.1.4 Near Isogenic Line (NIL) Pairs

Many studies have mapped disease QTL however the precision of these position estimates is limited [13]. To enhance the precision of QTL mapping and to confirm their effects, information from RILs can be analyzed along with near isogenic line pairs (NILs). A NIL pair has a uniform genetic background that differs only at a specific region of interest. In this way, NILs are useful for focused studies on the effects of individual QTL. They are developed through repeated backcrossing that is sometimes marker assisted to confirm the presence of the target. For maize, NIL pairs have been developed to study natural variation [14].

1.2 *Cochliobolous heterostrophous*

The Fungi kingdom is large and diverse. The genus *Cochliobolous* contains many species and subspecies that are pathogenic to cereal crops such as maize, wheat and rice [15,16]. *C.heterostrophous* is the causal fungus of the foliar disease Southern Leaf Blight (SLB). It survives well in warm, moist environments making it problematic in the south half of the world, hence the name Southern Leaf Blight [15 17]. The life and disease cycle (Figure 5) have been documented. Sexual reproduction is rarely seen in the field but has been observed in culture [16]. The nomenclature of the

anamorph is *Bipolaris maydis*, named after the observation of germination from both poles of a spore and its contribution to the plight of maize crops. Spores are transferred aerially and can be carried in dust.

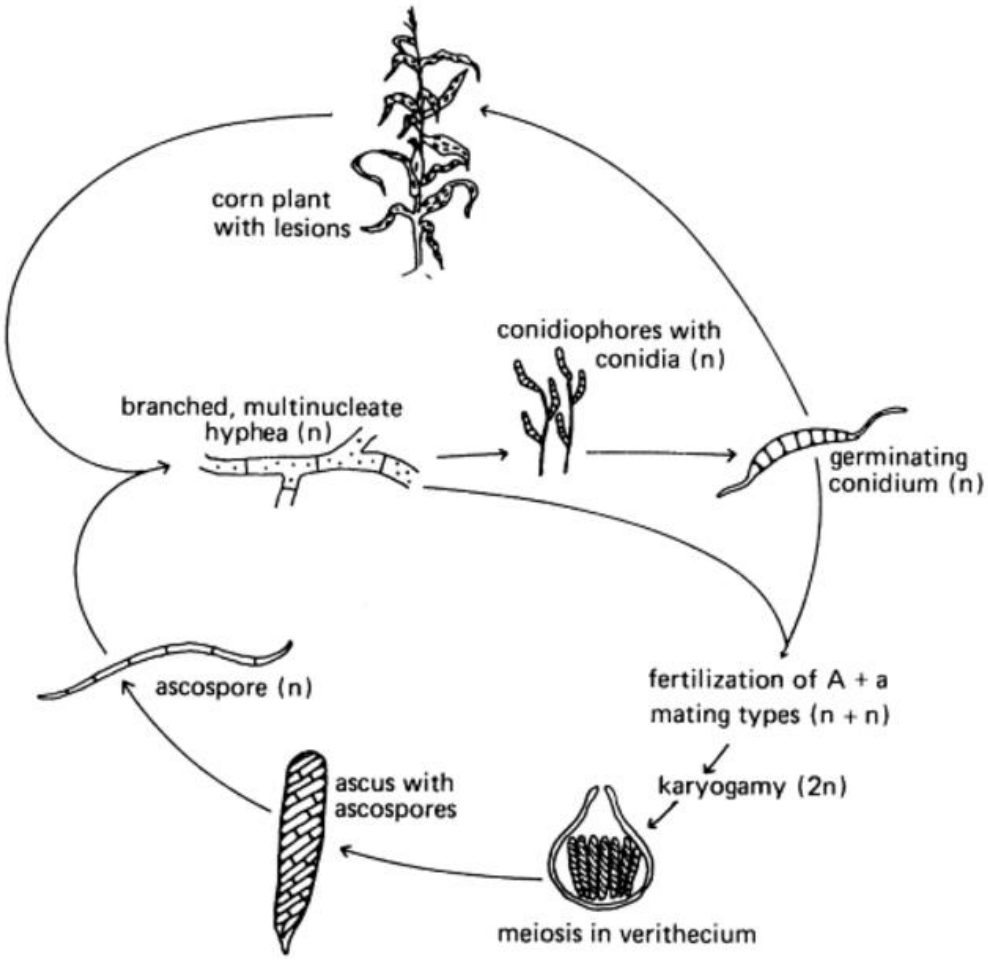

Figure 5 Life and disease cycle of *C.heterostrophous* (figure from Yoder 1988)

C. heterostrophous like many other necrotrophic fungi, produce host specific toxins (HSTs) that have a wide range of effects on plant tissue. Different races of the species *C.heterostrophous* carry genes that produce different toxins [17]. Successful methods for genetic transformation of *C.heterostrophous* have been established that aide in the understanding of these HST genes.

Symptoms of SLB include small, oblong, tan, irregularly dispersed lesions found on the leaf. These areas lose the ability to photosynthesize leading to diminished plant life. The disease progresses quickly with some greenhouse studies showing visible signs of disease as early as 24 hours past inoculation. Natural resistance varies greatly between inbred lines as seen in figure 6 [3].

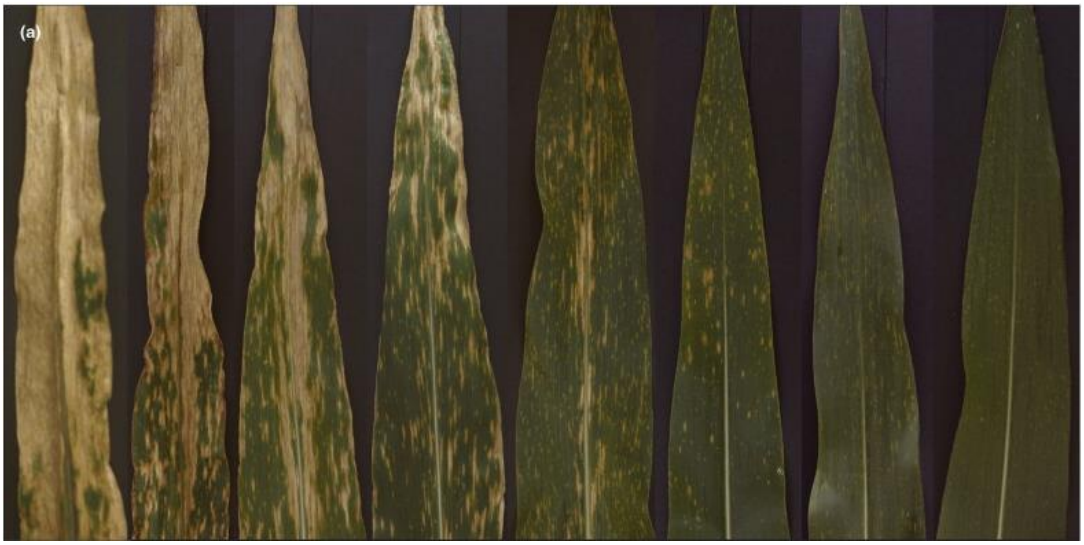

Figure 6 Maize lines of varying resistance showing symptoms of Southern Leaf Blight at the same time point (figure from Poland et al. 2009).

Microscopic studies of *C.heterostrophous* pathogenesis is limited and quite dated. One report published 1977 provided an account of some of the features of *C.heterostrophous* in maize leaves[18]. Wheeler describes seeing extended growth on leaf surfaces and along cell walls. All penetration events took place between epidermal cells or between a guard cell and a subsidiary cell. The fungus forms an "infection cushion" prior to penetration and frequently forms another one beneath the cuticle. Hyphae was seen growing abundantly from the secondary structure. Higher resolution imaging of *C.heterostrophous* can provide a more in depth understanding of these features.

1.3 Advances in Imaging

Some hurdles to resolving microscopic features have to some degree been overcome by advances in microscopy such as fluorescent laser scanning confocal and multi-photon imaging. These techniques have become increasingly popular as they confer the benefits of three-dimensional imaging [19,20]. As opposed to conventional two-dimensional light or electron microscopy, three-dimensional laser scanning confocal microscopy allows for in situ investigation of structures without physically sectioning and can be used for the identification and quantification of features of a specimen (such as topography, thickness, etc.)[20]. Confocal and multi-photon microscopy techniques have also been enhanced through utilization of fluorescent probes. Fluorescent proteins, fluorescently labeled antibodies and fluorescent stains allow for the differentiation of cellular and tissue structures making three-dimensional rendering and reconstruction of structures in specimens possible [6].

1.3.1 Fluorescence Microscopy

Fluorescence is the ability of a substance to be excited by photons of light, absorb the energy, and emit photons at a longer wavelength (Figure 7). Fluorescence microscopy takes advantage of this phenomenon through the use of specific stains, filters and dichroic mirrors. Light from either a mercury or halogen bulb travels through an excitation filter that is chosen based on the size of the desired wavelength. Light then reflects off a dichroic mirror placed at a 45° angle through the objective and onto the specimen. Dichroic mirrors can only reflect specific wavelengths, enabling longer wavelengths to pass. The light from the specimen is now collected through the objective and passes through the dichroic mirror to an emission filter. This filter excludes light of other wavelengths from passing through to the eyepiece or detector, ensuring that only the anticipated wavelength is observed [21].

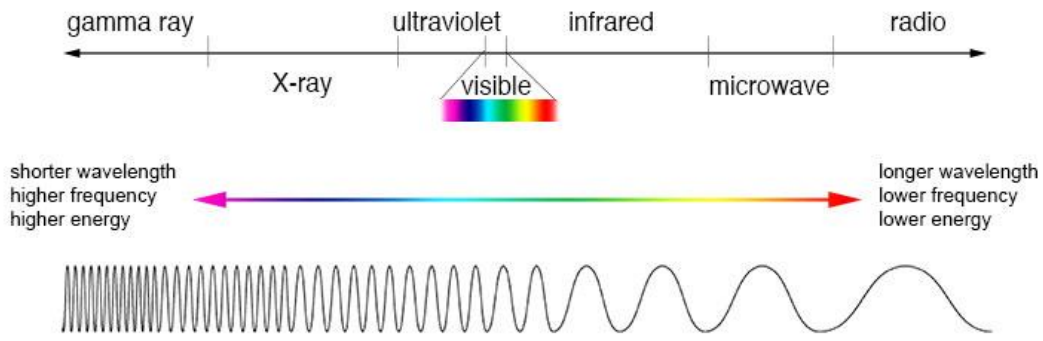

Figure **7** Electromagnetic spectrum

Jablonski described how molecules can reach an excited state and emit at a lower wavelength in a useful diagram. His diagram demonstrates how incoming light

is absorbed by electrons, raising the energy from the ground state to an excited state. The electrons enter a relaxed state and lose small increments of energy. Electrons returning to the ground state produce light. Fluorescent molecules emit light at a higher wavelength than that used to excite it. This is due to the loss of vibrational energy when electrons go from an excited state to a ground state. The shift on the spectrum between the excited and emitted wavelengths is known as the Stoke's shift (Figure 8). A larger gap in the shift makes it easier to discern between the excited light and emitted light.

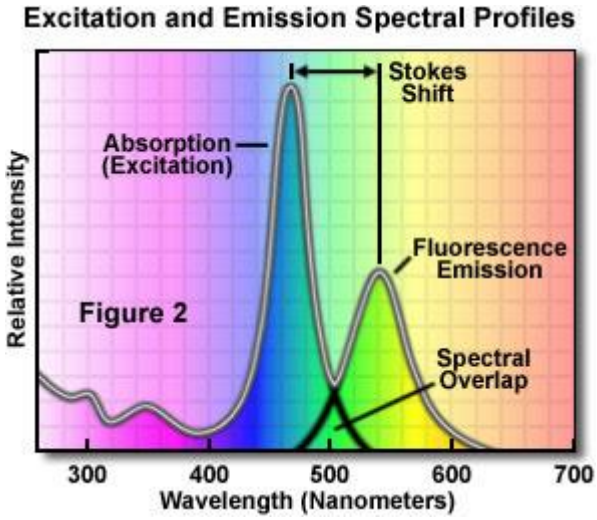

Figure 8 Stokes shift

1.3.2 Confocal Microscopy

The advantages of fluorescence microscopy can be further exploited with the use of confocal microscopy. Marvin Minsky is credited with inventing the confocal microscope [22]. His design uses a point source of light focused through an objective to illuminate a specimen, light emitted from the sample will be collected by the same

objective before being focused on a pinhole to exclude scattered light from other focal planes. The pinhole and focal point lie on conjugate planes giving rise to the name 'confocal' [23]. This principle coupled with a moving stage allows users to image with great resolution through thick specimens.

Laser scanning confocal microscopy builds on the basic confocal principle with the use of high powered and easily controllable lasers to excite fluorescence. High power lasers increase the signal to noise ratio but can also cause photo bleaching and other detrimental effects to the sample. Different types of lasers excite at different wavelengths and laser strength can be adjusted to reduce sample bleaching.

A much faster alternative to the point scanning confocal method is the line scanning confocal system. Using a line scanning in one direction as opposed to a point focus greatly improves the collection of frames per second [24].

1.3.3 Multiphoton Microscopy

Multiphoton microscopy eliminates the need for a pinhole by using two-photons to excite at the same point [25]. By using a pulsed laser emitting a wavelength approximately twice as large as the wavelength necessary to excite a particular fluorophore, the combined energy of both wavelengths will excite specifically where it is focused. No out of focus light is produced maintaining resolution in deep samples.

1.3.4 Sample Clearing

Although fluorescent imaging techniques have been widely applied to plant imaging, some challenges remain. One of these challenges is that depth of fluorescent imaging in plant material is often obstructed by light scattering molecules present in the cuticle, vasculature and mesophyll tissues [26]. Despite the fact that multi-photon

imaging generally can penetrate deeper into tissue, clearing of these light scattering molecules is still necessary to achieve optimal and fully traverse imaging. Chemical clearing agents such as the traditionally used chloral hydrate and recently established Sca*l*eP [27] and other methods [26,28] have been shown to increase transparency in plant tissue and improve three-dimensional imaging quality. The increase in imaging resolution of three dimensional structures is especially valuable during investigation of plant-pathogen interactions as spatiotemporal associations between organisms can be elucidated [6].

Chloral hydrate has been reported as a successful clearing agent however it is a restricted chemical and alternative clearing agents have been reported that are accessible. KOH, methanol and Visikol have all been reported as clearing agents and were tested for this project [29–31]. Other clearing agents such as 2,2′-thiodiethanol (TDE), ethanol, acetic acid and acetone were attempted with limited investigation or success.

1.4 Fungal Quantification

Most microscopy investigations can collect only a limited amount of information which is not enough to compare quantitative traits. To sufficiently analyze disease resistance statistical inference is needed from an abundant amount of fungal events. Imaging platforms to quickly observe large samples in depth and the cyberinfrastructure to compute and store these datasets are critical for measuring and comparing phenotypes [6].

Accurately quantifying fungal biomass is important in measuring disease resistance. Many of the methods currently in place to score susceptibility to disease is

subjective [5]. A technique to quantify and compare biomass by way of detecting the fungal cell wall component, chitin exists however tissues for this method must be homogenized [5]. In the field, scientists may measure lesion size or attempt to estimate the amount of visible fungus present. Hyphae that spread within a leaf tissue are not easily visible to the naked eye and are left out of these estimates. Confocal microscopy has long been chosen to evaluate features of pathogenesis in plants [20,30,32]. Practical methods for quantifying macroscopic fungal data in microscopic detail have been described in detail by Minker et al and will be discussed further in later chapters.

Chapter 2

MATERIALS AND METHODS

2.1 Selected Maize Lines

Two maize lines, B73 and Mo17 were chosen for this study. The lines represent different extremes in susceptibility to SLB. 309 lines were robustly phenotyped ranking B73 and Mo17 258th and 22nd respectively in resistance. The full genome of B73 has been sequenced [8] and a similar resource for Mo17 is being developed. Populations of B73 and Mo17 were used in this project in conjunction with NAM [11]. Several QTL have been mapped using a family of inbred lines that were derived from crosses of B73 and Mo17 [3,13,33]. Profiling the expression and quantifying features of these two parental lines will therefore provide insightful details on the variation in disease progression between susceptible and resistant inbred lines relevant to the maize research community.

2.2 Sample Inoculation, Collection, and Fixation

Maize inbred lines B73 and Mo17 were grown in growth chambers under long-day light conditions (16 hours light/8 hours dark). Temperatures within the chambers were maintained at 25 ˚C during the light period and 18˚C during the dark period. Inoculation was carried out 21 days after planting. For *C.heterostrophous* plants were spray-inoculated at the fifth leaf with 5×10^4 spore solution that consisted of *C.heterostrophous* spores suspended in a chilled solution of 0.05% agar and 0.05% Tween 20. The plants were allowed to dry for 30 minutes and then placed in clear plastic bags for approximately 16 hours overnight, after which the bags were removed. Leaf samples were collected at 12, 24 and 48 hours post inoculation.

Leaf tissue was excised using a 14 mm square punch and placed into 24-well tissue culture plates containing 2 mL of 2% glutaraldehyde, 2% paraformaldehyde, and 0.05% Triton X-100 in 1X PBS pH 7.4. During sampling, plates were kept on ice. The following procedure was used to ensure an even distribution of fixative within the tissue samples and to remove air pockets. Weights (e.g. balls of aluminum foil) were placed over each leaf sample such that it remained submerged in solution (Figure 9). Plates were transferred to a bell jar and incubated under vacuum at 30 inHg for 3 hours. The weights and fixative solution were discarded, and each well was replenished with 2 mL 1X PBS and a new weight. Samples were incubated under vacuum at 30 inHg for an additional 18 hours, then rinsed three times with 1X PBS to remove residual fixative solution. At this stage in the protocol, samples that float in solution may still contain air pockets and require a longer incubation under vacuum. Plates were sealed using parafilm and kept at 4 °C [6].

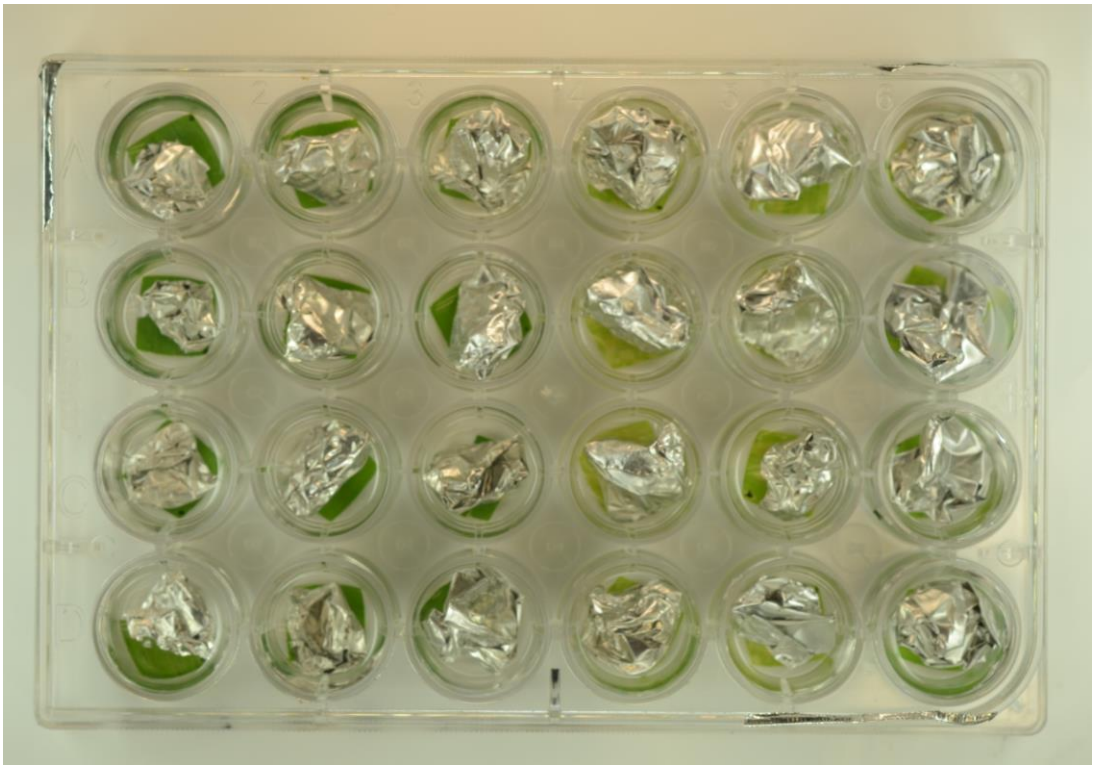

Figure 9 Samples in 24 well plate under weight of foil balls.

2.3 Clearing

Microscopy depends on the passage of light through a sample. The refractive properties of cellular components, as well as the thickness of a given sample contribute to the ability, or lack thereof, to visualize through an entire sample. Warner et al (2014) describe a technique for clearing plant material that was modified from another clearing technique applied to mouse brains called Sca*l*e [34]. Sca*l*e for plants, or Sca*l*eP [6], is a mixture of 6m urea, 30% (v/v) glycerol, and 0.1% Triton X-100. The effect of Sca*l*eP alone is not enough to clear through the entire depth of the leaf (Figure 10). This in combination with a12 hour pre-treatment of 10% (wt/vol) KOH

allowed for full depth of clarity throughout the entire leaf tissue while leaving all cellular structures in tact (Figure 11).

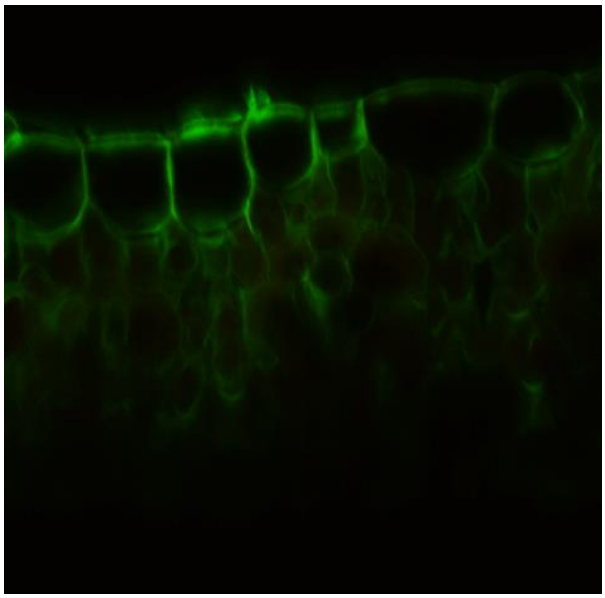

Figure 10 Cross section of maize treated with Sca*l*eP only. Imaged at a depth of 220 µm

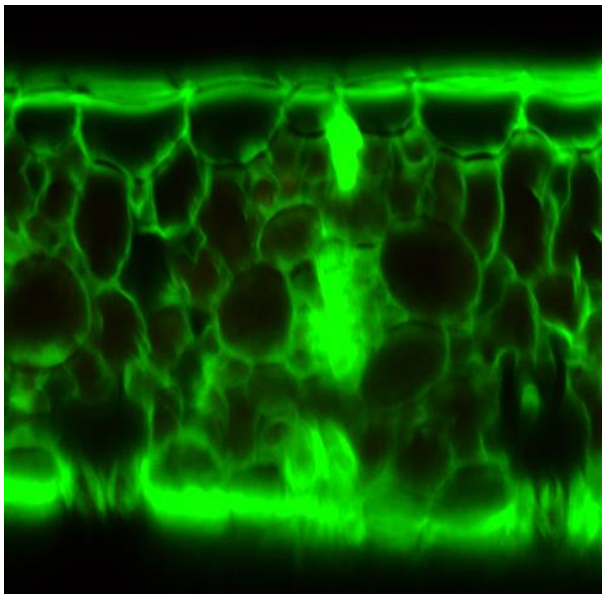

Figure 11 Cross section of maize treated with KOH and Sca*l*eP. Imaged at a depth of 220 µm.

KOH pretreatment was followed by rinsing three times in 10x PBS. Samples were then incubated in 0.2M glycine for 18 hours. The addition of glycine quenches autofluorescence that is caused by left over fixative. A demonstration of the effect of glycine is seen in figure 12 of a maize leaf infected with *S.turcica*.

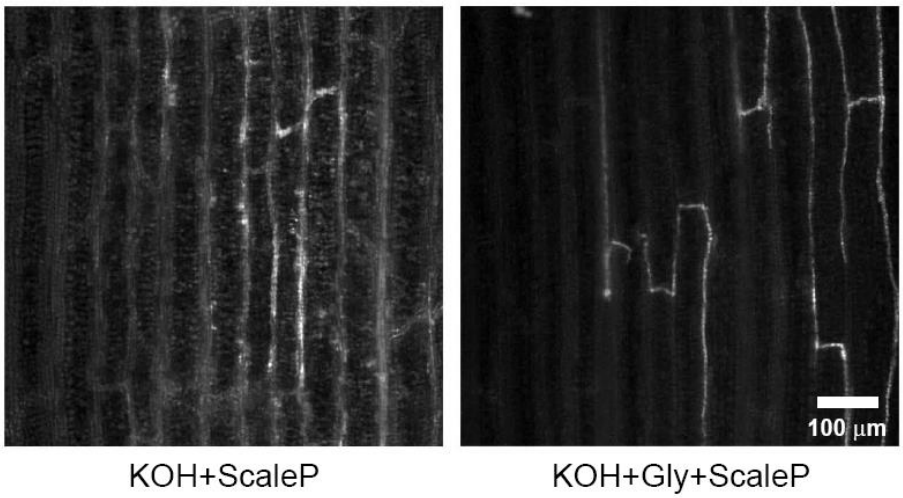

Figure 12 Effect of glycine. Two different samples with *S.turcica* infection. Signal to noise increases with treatment of 0.2M glycine.

2.4 Staining

Samples were incubated for five days in a mixture of 1.09 mM Calcofluor White MR2® (CW; Sigma-Aldrich, St. Louis, MO) and 0.026 mM wheat germ agglutinin conjugated to Alexa Fluor® 568 or 594 (WGA-AF568/WGA-AFF594; Thermofisher Scientific, Carlsbad, CA). Their emission spectra are easily separated on most fluorescent microscopes, including laser scanning confocal microscopes. Furthermore, a common multiphoton excitation wavelength (745-760 nm) can excite both CW and WGA AF594. Although CW stains both plant and fungal cell walls, it is nearly impossible to distinguish between the plant and fungi based on structure alone. Therefore, it is essential to specifically stain the fungi. WGA provided high specificity, which was surprising since it reportedly binds any sialic acid or N-acetylglucosaminyl residues [35]. Since it is also widely used to stain the plasma membrane, it was quite unexpected that it did not stain the plant tissue. Interestingly, WGA has been used previously to detect fungi in resin embedded and sectioned

samples using standard electron microscopy protocols [32]. It is reported to be very specific to a fungal cell wall component, chitin. Another significant advantage of using WGA over other dyes is that it can be conjugated to dyes with varying fluorescent properties. Since it is the most widely used lectin in microscopy, blue, green, red and far-red dye conjugates are readily available. WGA conjugated Alexa Fluor® Alexa Fluor® 594 (WGA-AF594) [6].

2.5 Highspeed Confocal

Laser scanning confocal microscopy was conducted on a Zeiss LSM5 DUO (Carl Zeiss, Inc) using the LIVE Line-scanning scanhead. 405 nm and 561 nm laser lines were used to detect CW and WGA-AF594 respectively. Fluorescence emission was collected with a band pass of 415-480 nm for CW and 575-615 nm WGA-AF594 respectively. Tile scans (10 x 10) were collected with a pinhole of 10 μm and gain values between 3-5 on the linear charged coupled device camera. Image size was 256 x 256 pixels with 4X binning and 0.5X zoom. Z-interval size was 1.2 μm for 150 z-slices with a fast piezo objective nanopositioner (Physik Instrumente, Auburn, MA) [6]. A macro for Zeiss 2009 called MultiTime (v20) was used to set up overnight imaging of multiple samples.

2.5.1 Magnification

Three objectives were examined including a 5X Fluar with a 0.25 Numerical Aperature (NA), a 10X Planapochromat (0.45 NA) and a 20X Planapochromat (0.8 NA). Data collected at 20X provides remarkable improvement in Z resolution without too much compromise in other imaging aspects and will be discussed further in the next chapter.

2.5.2 Shading (method from Abhishek Kolagunda; UD, CIS Ph.D. candidate)

The illumination profile of the highspeed confocal microscope that was used to collect data changes frequently. This causes shading artifacts in each image tile that interfere with image quality. This can be corrected by collecting a reference image of a light profile for each band pass. An algorithm was designed specifically for this project that applies the light profile to each tile to equalize intensities (Figure 13).

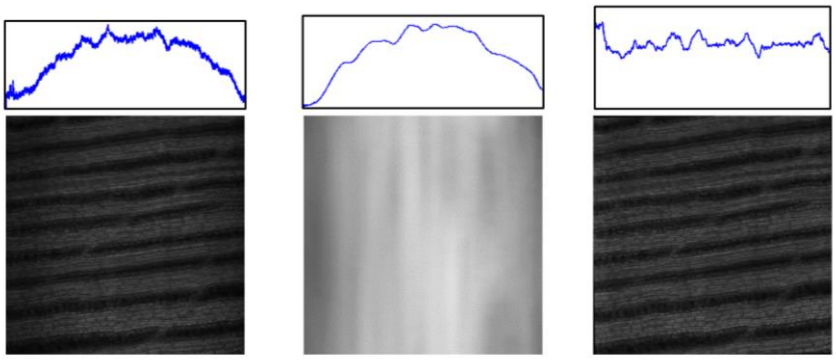

Figure 13 Shading correction. Tile before shading, reference image of illumination profile, corrected tile. The intensity profiles for each image are displayed.

2.5.3 Stitching (method from Abhishek Kolagunda; UD, CIS Ph.D. candidate)

Stitching was performed using Fiji [36]. The source code of the stitching grid plugin by Preibisch et al [37]. (2009; downloaded on 12/19/2013 from: https://github.com/fiji/Stitching/tree/master/src/main/java/plugin/) was modified to be server compatible (GUI independent), to improve stitching accuracy and efficiency, and to append metadata to the reconstructed image.

To improve stitching accuracy, the algorithm was modified to prevent alignment between tiles at different locations in Z; at each location along Z, phase correlation was applied only to data at the same depth location. This modification

prevents errors in Z alignment, assuming no Z-offsets have occurred when imaging different tiles. Furthermore, translation estimate errors (now, only XY alignments) were minimized by constraining translation between tiles according to the percentage of overlap used to image neighboring tiles (here, 8%).

Stitching speed was enhanced by taking advantage of the known grid structure for this data set and used only those tiles expected to be contributing to a center pixel. In our case, this minimized the search space to the nine neighboring tiles instead of all 100 tiles.

A script was developed by Abhishek Kolagunda for tiling samples from an inventory spreadsheet linked to the data. As images are generated, manual entries are made in an excel spreadsheet that indicate the name of the sample and the tiles that correspond to it. A graphical user interface button was created to initiate tiling.

2.5.4 Iterative Template Matching (method from Abhishek Kolagunda; UD, CIS Ph.D. candidate)

Predictable features of the leaf such as stomata can be quantified computationally through computer learning. Fungal spores appear as part of the leaf channel because WGA AF594 does not bind to it. Its distinct shape enables computers to learn it, and filter it. Manually marking spores and recording measurement information about them was necessary to give a basis for the computation. Features of the image are extracted before templates are applied to detect spores.

2.5.5 Maximum Intensity Projection (MIP) (implemented by Abhishek Kolagunda; UD, CIS Ph.D. candidate)

For fungal analysis 3D data was converted to a maximum intensity projection (MIP). MIP projects voxels with a maximum intensity value from every slice to a 2D

image. This is a necessary precursor step for any further downstream analysis. MIPs are also useful when gauging the amount of fungal presence by eye.

2.5.6 Skeletonization (method from Stephen Rhein; UD former CIS Ph.D. candidate)

Image analysis of large networks of hyphae can be difficult when looking at raw data. Hyphal networks can be very complex and seemingly random in directionality and thickness to non-biologists. An algorithm to simplify strands was developed by Stephen Rhein for this project that provides a pruned skeleton of the network while still preserving information about hyphal width.

To compute hyphal width, a set of values are assigned to hyphae in the MIP. Small values correlate to scores for fungal gnarly-ness while larger values are a score of curvilinear regions. Thresholding the scores segments likely hyphal locations in the image. Gnarly-ness scores give more confident locations due to the behavior of the fungus, some of the curvilinear scores may potentially be noise caused by structures of the leaf. Using a computer science procedure called multi-modal hysteresis, the gnarly junctions that were scored are connected to strands scored in curvilinear. A transformation is applied that skeletonizes the segmented hyphae that also calculates the width of the hyphae in pixels. This measurement is multiplied by the resolution of the captured image to compute the physical width.

To further eliminate any noise from the skeleton an algorithm for pruning skeleton leaves was applied. Once the width for a connecting node is calculated, leaves that have a distance from their connecting node that is less than the width of the node are pruned.

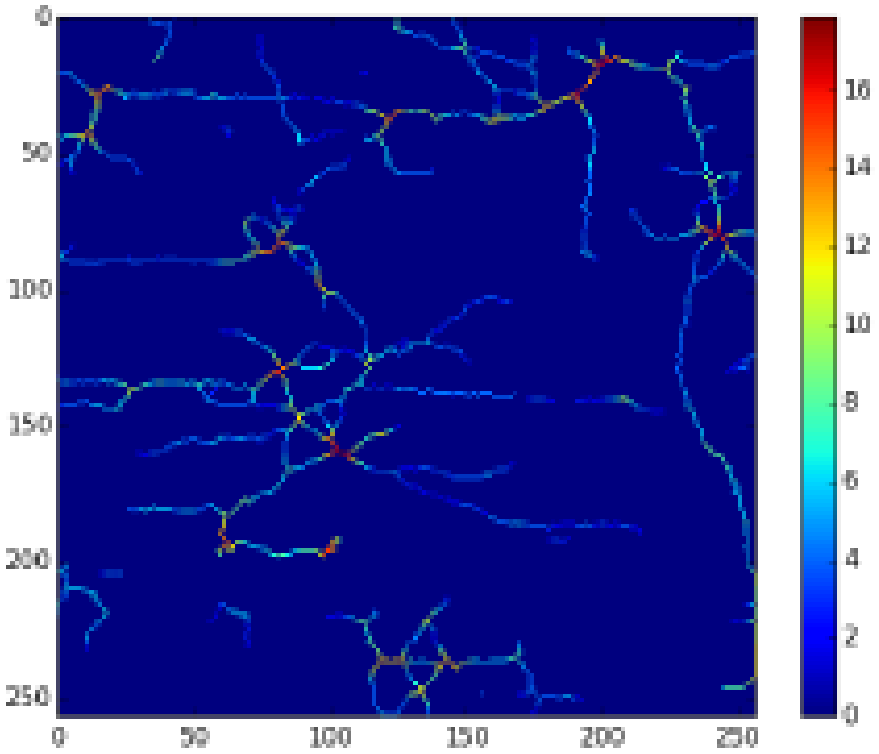

Figure 14 Skeleton heat map indicating hyphal width

2.6 Multiphoton Microscopy

Multiphoton microscopy was conducted on a Zeiss LSM510 NLO or Zeiss LSM880 NLO equipped with a 5W Verdi pumped Mira (Coherent Inc, Santa Clara, CA) multiphoton tuned to 745 nm. Comparison of single-photon and multiphoton excitation was conducted on a Zeiss LSM780 with a Chameleon Vision multiphoton tuned to 760 nm. 405 nm and 561 laser lines were used to detect of CW and WGA-AF594 respectively. Fluorescence emission was collected with a band pass of 412-482 nm for CW and a BP 569- 648 nm for WGA-AF594. The z-interval size was 0.400 µm and image size was 1024 x 1024 pixels. Gain value of the GaAsP detector was 690 for both channels. Laser power was adjusted between 0.3% - 7.5% for the 405 nm laser,

1.8% - 15% for the 561 nm laser or 2.8% - 9% for the 760 nm multiphoton laser through the stack to correct for signal loss through the sample [6].

2.7 3D renderings using Amira

Multiphoton images were deconvolved using Huygens software (Scientific Volume Imaging, Hilversum, Netherlands) and the Classic Maximum Likelihood Estimation (CLME) algorithm. Images were then imported into Amira 6.0.1 (FEI, Hillsboro, Oregon) for 3D segmentation, volumetric rendering and surface rendering.

Chapter 3

RESULTS

3.1 Sample Mounting and Preservation

Usually immediately and no more than one day following incubation in 20% glycerol, samples were mounted between two 113 mm x 75 mm x 0.17 mm cover glass slips (cat. no. 70091137B; Live Cell Instruments, Seoul, South Korea), which are referred to as a slide. Each slide included either 12 or 24 samples arranged in a 3 x 4 or 4 x 6 format respectively. A black and white template was created that was the same size as the base coverslip, using black squares to represent samples with their ideal placement on a slide. With the template underneath the base coverslip, one drop of 20% glycerol was placed in the middle of each black square where samples were then carefully situated on the drop with the adaxial side of the leaf facing upward. Air bubbles that may have occurred between the sample and base coverslip were gently pushed away using forceps. Additional drops of 20% glycerol were added on top of and between samples until the slide was saturated, but not flooded. The top coverslip was cut to a custom size following a template using a diamond scribe. The coverslip had to be large enough to cover the samples but slightly smaller than the base coverslip to allow room for sealing. The top coverslip was placed down gradually from one long-edge to the other to minimize the introduction of air bubbles. The edges of the slide were wiped dry and sealed with clear nail polish. Mounted slides were placed in the dark and stored in a refrigerator to maintain fluorescence and sample stability [6].

Samples are mounted in 20% glycerol as opposed to Sca*l*eP for several reasons: Before sealing slides with nail polish they were initially sealed using a

Chamlide magnetic system (Live Cell Instruments) and VALAP (vasoline lanolin paraffin) on a hot plate to rapidly seal the samples. However, due to the flexibility of the large cover glasses the seal was easily broken causing the urea in the Sca*l*eP to crystalize and damage samples. While great improvements have been made by sealing slides with nail polish, occasionally this seal is insufficient and samples can dry out or potentially crystalize. The refractive indexes of 20% glycerol (1.364) and Sca*l*eP (1.369) are very close, differing by only .005. Changes in imaging protocol would be very minimal should a need arise to mount samples in Sca*l*eP. No loss of clearing effect was observed by removing samples from Sca*l*eP.

3.2 Establishment of a Semi-Automated Platform

A major challenge of analyzing fungal infection in maize tissue is the large, millimeter-scaled expansion of infection compared to the small, micrometer-scaled interactions and features, such as penetration by the pathogen into host cells, branching of hyphae during pathogen invasion and distribution of hyphae resulting from pathogen colonization in different tissue layers. In general, capturing multiple scales of detail in a way that the data can be correlated and analyzed unbiasedly with computational tools is a major challenge in microscopy [6].

A pipeline to generate a medium throughput of image data was developed as a result of this project. Techniques for mounting multiple samples on large pieces of cover glass coupled with great computational power enabled much of the data collection to be automated. The methodologies include sample fixation, clearing, staining, mounting, confocal imaging, computational stitching of images and image analysis (Figure 15). We have optimized these methods to create an efficient workflow for multi-scale 3D analysis of multiple organisms or structures within a specimen

sampled from across a time course (4D). Each method within the platform has the potential to be co-opted for a variety of plant imaging applications, and therefore, can be broadly used by the research community [6].

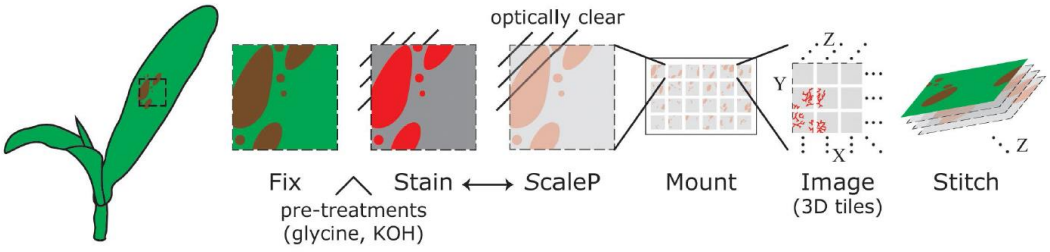

Figure 15 Macroscopic microscopy workflow

3.3 Magnification Compromises

Medium to large scale imaging is often a balance between resolution and speed. To determine what X, Y and Z resolution was required for our study, I examined the resolution of three microscope objectives with different magnifications and numerical apertures. I chose a 5X Fluar (0.25 NA), a 10X Planapochromat (0.45 NA) and a 20X Planapochromat (0.8 NA) for this analysis. Lower magnifications allowed faster imaging of larger areas at the expense of resolution. All objectives resolved hyphal networks and plant structures, such as guard cells, in XY (Figure 16A). For analyses that do not require 3D information, 10X magnification seemed to be an excellent compromise between field of view and resolution. For this study we needed to capture the 3D distribution of plant-pathogen interactions. Examination of XZ cross-sections through hyphae with the three objectives showed that the 20X Planapochromat (NA 0.8) was required to resolve the location of hyphae in 3D and to

resolve both the adaxial and abaxial surfaces of the leaf. Furthermore, individual hyphal strands could be resolved in Z with 20X but not the 10X objective (Figure 16B-C). Analysis of fungal width distributions from 20X data indicated that a pixel resolution of ~1.2 μm can resolve the majority of hyphae, but the sparseness of hyphal growth may permit imaging at a lower resolution, particularly for analysis of hyphae at the 2D-XY millimeter scale.

The requirement of a 20X Planapochromat (NA 0.8) for axial resolution meant that a large grid of tiled images was required to cover a sufficiently large area of the sample. The central region of each 14 mm^2 leaf sample was captured in a 10 x 10 grid of image tiles, representing a leaf area of 6 mm^2. Each tile contained 150 z-slices to capture the full depth and contours of the leaf. To collect this large amount of data in a short period of time, we chose a line-scanning confocal microscope (Zeiss LSM5 DUO) that can operate at up to 120 frames per second, full frame. The system was fitted with a high speed piezo motor objective positioner, a requirement for fast imaging of 150 z-slices. For each tissue sample, CW (plant) and WGA (fungal) channels were imaged across the 10 x 10 grid comprising 30,000 images that could be collected in approximately 30 minutes. Although we used a high speed, line scanning confocal microscope for image acquisition, it is possible that other fast 3D imaging systems can be used; this includes resonant point scanning confocal microscopy, spinning disk confocal microscopy, wide-field fluorescence microscopy with deconvolution and fluorescent slide scanning systems [6].

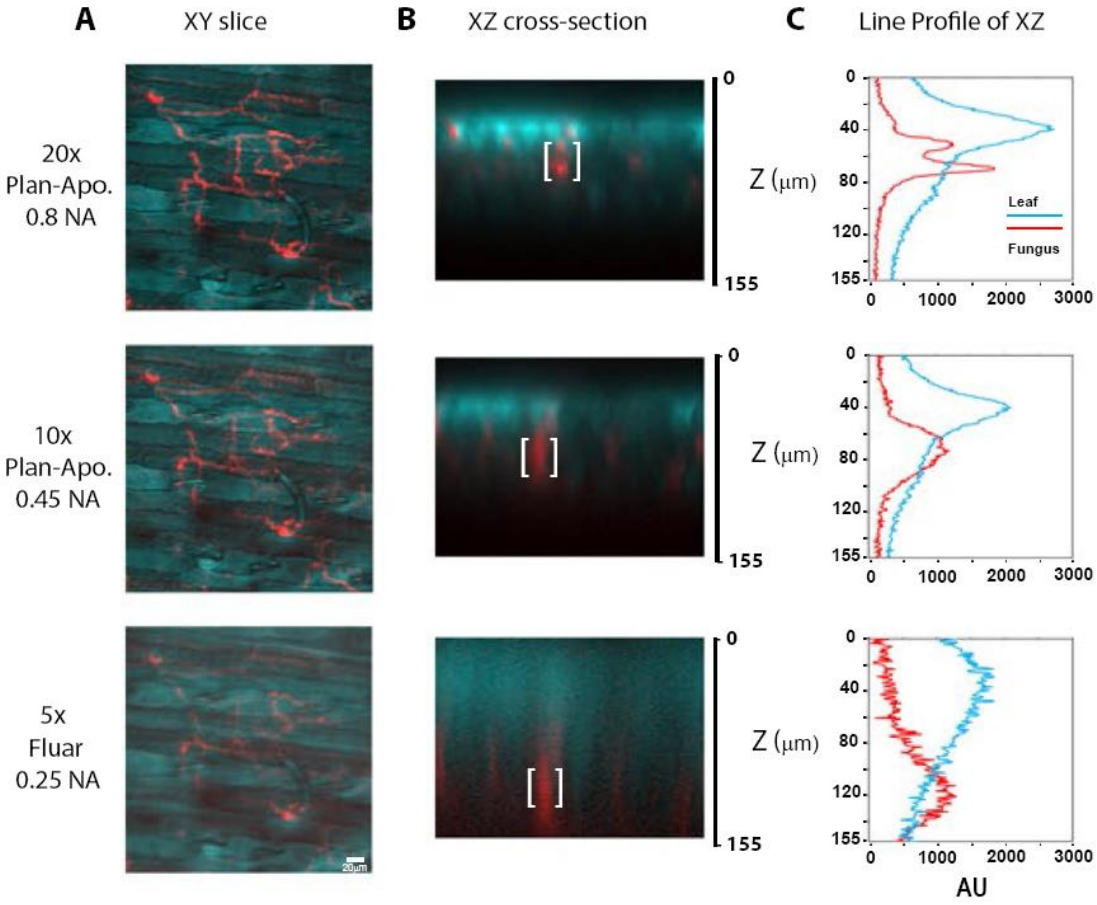

Figure 16 Magnification comparison **A**. The same sample was imaged at a depth of 155 µm using 20x Plan-Apochromat 0.8 NA, 10x Plan-Apochromat 0.45 NA, and 5x Fluar 0.25 NA. The zoom for 10x and 5x objectives were adjusted to match that of 20x. Maximum intensity projections (MIP) of the fungal channel (red) reveals there is minimal difference in XY fungal detection (red) using 20x and 10x objectives. Image quality decreased with 5x. **B**. A cross-section taken at the same point shows the dramatic difference in resolution between each objective. **C**. A signal profile of the bracketed area in 20x shows two peaks, distinguishing that there are two separate hyphae at different levels of deepness. The profiles of the same area imaged with both the 10x and 5x objective show that the signal between those two strands could not be separated. Profiles of the leaf channel for both 20x and 10x show clear peaks that correspond with the upper leaf surface.

3.4 Quantification of Fungal Mass; B73 vs Mo17

Three plants from each inbred line were randomly selected at twelve, twenty four, and forty eight hours past inoculation (hpi). Five leaf samples were collected from the fifth leaf of each plant. One sample is used to validate gene expression with RNA-Seq, leaving the other four for imaging. For each sample one hundred images are collected in a 10x10 grid that when tiled together cover approximately 6mmx6mm of the center. The following information was attained from skeletonization data from a set of samples referred to as experiment 13.

Pixel information for skeletons in each tile was calculated and subtracted from the total number of pixels in the tile to determine size of the leaf area. Skelton details such as number of nodes, leaves, or edges were recorded. Comparisons of these features can easily be done using a cumulative distribution function to display the proportion of tiles that contain a percentage of hyphae (nodes, leaves, edges, etc.) or less.

First, we quantified the total amount of hyphae found on B73 and Mo17 at twelve and forty eight hours past inoculation (Figure 17). At twelve hpi, about 80% of tiles in both B73 and Mo17 have the same amount of hyphal coverage. A noticeable difference between the susceptible B73 and resistant Mo17 is seen this early in pathogenesis and becomes more obvious in the forty eight hour time point. All tiles from twelve hpi presented less than 0.025% hyphal coverage. Mo17 at forty eight hpi had a large proportion of tiles that fell under 0.025% indicating effective resistance. B73 in contrast has a large proportion of tiles that have almost twice as much hyphal coverage than the average Mo17 tile.

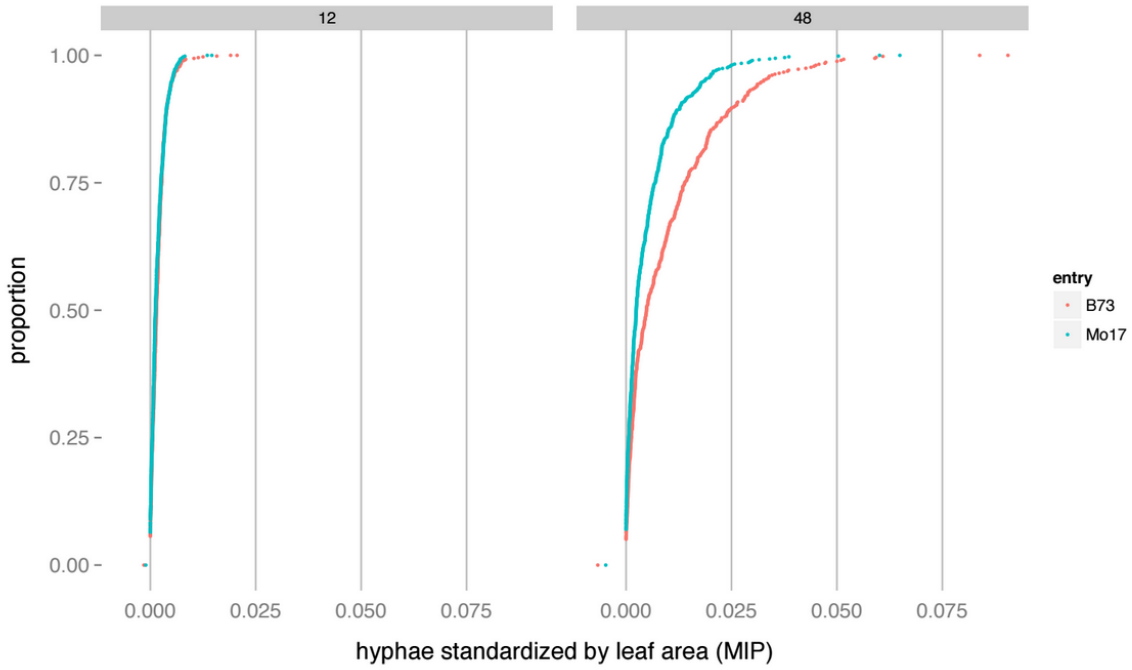

Figure 17 Hyphal presence at different time points. X-axis; amount of hyphae standardized by leaf area represented as a percentage. Y-axis; Proportion of tiles containing a corresponding percentage or less.

Branching is known to occur often in *C.heterostrophous*, each branch point in the skeleton is known as a node. Figure 18 shows two quantifications for node count in experiment 13 that can be interpreted in a biological context very differently. The first plot shows the total number of nodes on a tile standardized by its leaf area. It is clear at forty eight hpi that B73 has a larger proportion of tiles with a higher node count than Mo17. This difference in B73 is likely correlated with the higher proportion of tiles presenting more hyphal coverage in a leaf area than in Mo17. The second plot shows the proportion of tiles that contain a given number of nodes on its skeleton. In this way growth patterns such as straight versus gnarly can be interpreted.

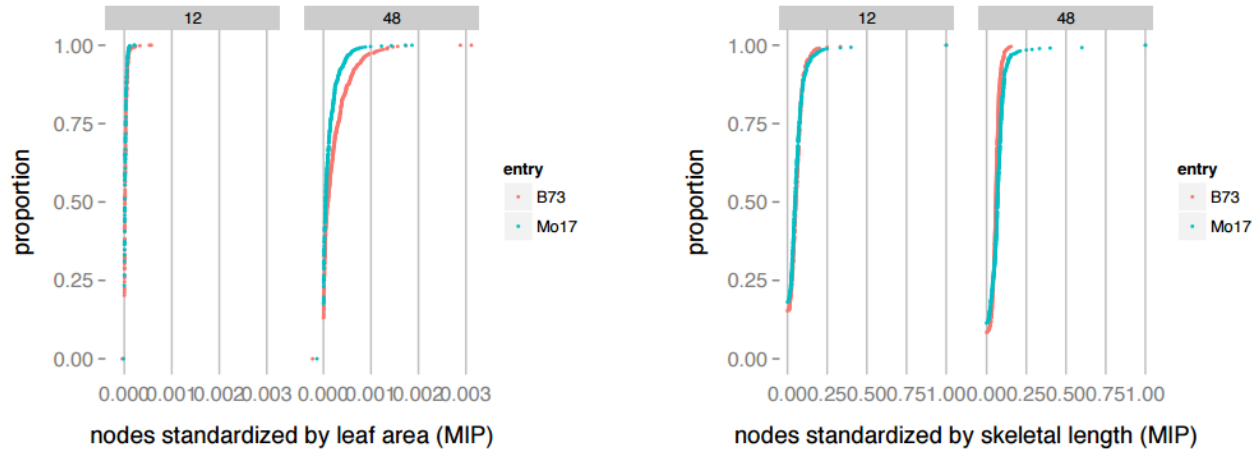

Figure 18 Quantification of hyphal nodes**.** X-axis left plot; percentage of skeleton that is considered a node standardized by the amount of leaf area. X-axis right plot; percentage of skeleton that is considered a node standardized by the length of the skeleton. Y-axis both plots; Proportion of tiles containing a corresponding percentage or less.

Two branch points are connected by a stretch of hyphae referred to as an edge in image analysis. Edges were quantified in the same fashion as nodes were quantified above and again, two different biological interpretations can be made. Edges standardized by leaf area show a similar trend between the two lines as the nodes did under the same standard. Again, the higher presence of hyphae on B73 is likely a contributing factor to the difference in edge presence. The plot of edges standardized by skeleton length shows a different tendency compared to the plot of nodes standardized by the same. At twelve hpi there is a slightly larger proportion of tiles with a high percentage of edges, which cannot be said about nodes at the same time point. This may suggest more of the nodes are connected to each other in B73 than in Mo17. At forty eight hpi the gap between B73 and Mo17 widens confirming that more

of the nodes are connected. Hyphae in B73 grow in a net like formation to maximize its surface area within the leaf tissue.

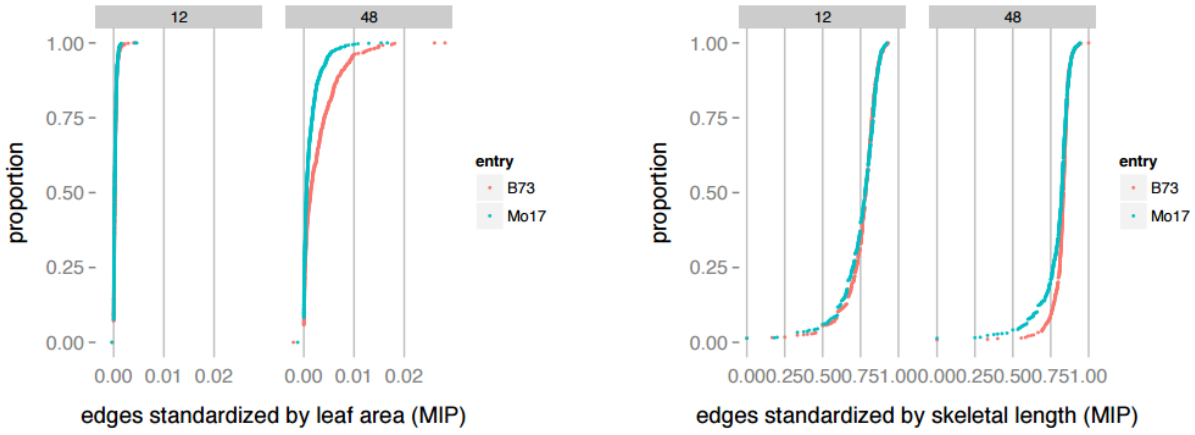

Figure 19 Quantification of hyphal edges. X-axis left plot; percentage of skeleton that is considered an edge standardized by the amount of leaf area. X-axis right plot; percentage of skeleton that is considered an edge standardized by the length of the skeleton. Y-axis both plots; Proportion of tiles containing a corresponding percentage or less.

All time points for experiment 13 were quantified in 2D and are displayed in below in Figures 20 and 21. I present the data similar to the above cumulative distribution plots however, each point is an entire sample rather than a single tile, thus the plots appear more staggered. Hyphal area standardized by leaf area represents a percentage of how much fungal presence is identified a defined leaf area. Hyphal length is the simplified, one pixel width, length of the entire skeleton. These plots indicate that fungal presence on B73 is much higher than on Mo17 and both plots trend in a very similar fashion.

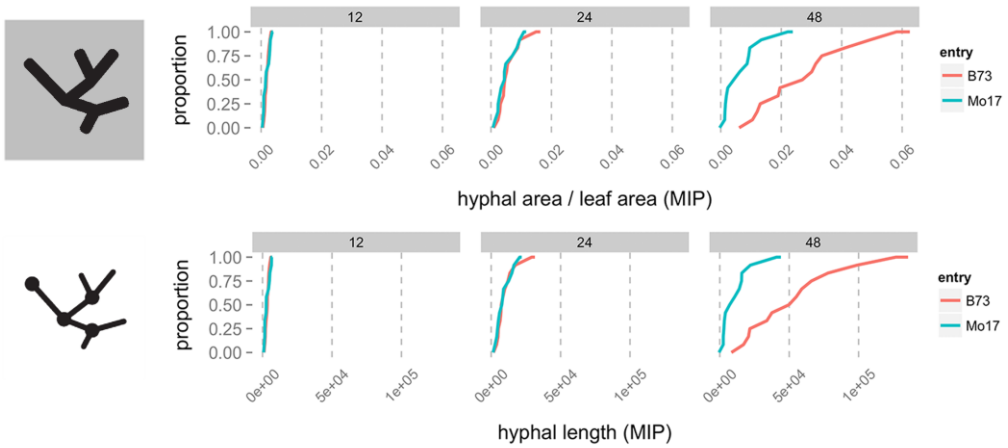

Figure 20 Hyphal quantification of all time points. X-axis for all plots is a percent. Y-axis is a proportion of samples with a given percent or less.

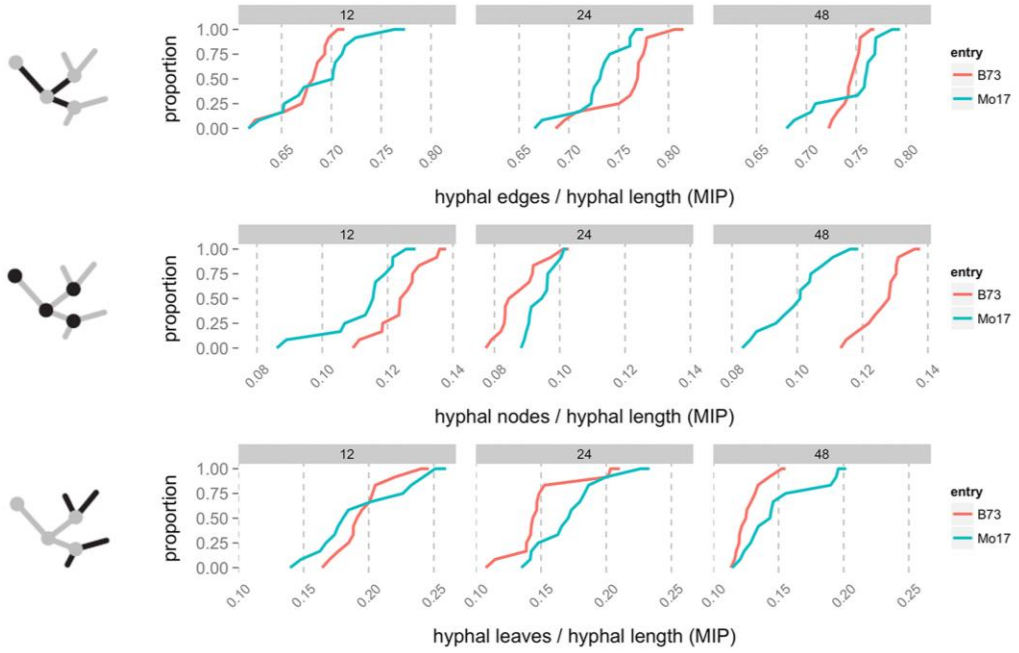

Figure 21 Quantification of pathogenesis features of all time points. X-axis for all plots is a percent. Y-axis is a proportion of samples with a given percent or less.

Mo17 has fewer nodes, more leaves, and at least half the samples at 48hpi have fewer edges than seen in B73. These numbers could suggest that mycelia in B73 are more successful at forming connections. Another possible interpretation is that Mo17 has more secondary branching and therefore more leaves per node as compared to hyphae in B73. The success or failure of this pathogen to progress throughout the leaf tissue is dependent on the cellular morphology of the leaf.

The above plots show similar tendencies as the plots of tile proportions (with the exception of nodes/skeletal length 48hpi). The plots showing the difference in number of leaves may validate the hypothesis that *C.heterostrophous* is more able to

reconnect with itself in B73 than in in Mo17. Leaves are described as fungal branches that are only connected to one node. It is likely that many of the connections are being made in the open space of the mesophyll indicating that cellular morphology and organization play a major role in disease resistance.

3.5 Pathogenesis in 3D

Infection begins when a spore lands on a leaf and germinates. *C. heterostrophous* is known to germinate from both ends of a spore (Figure 22) and proceed to grow on a leaf surface (Figure 23). Hyphae enter the leaf tissue by forming a small peg aided by pressure from the appressorium (Figure 24). Penetration events occur most often between epidermal cells (Figure 25C) or between a guard cell and a subsidiary cell (Figure 25A). Some events are intracellular but are generally contained to the cell in which it penetrated (Figure 25B) and does not spread much beyond that. The least observed form of entry was through the guard cells (Figure 25D), which would be a logical place for hyphae to enter considering they are openings to the leaf.

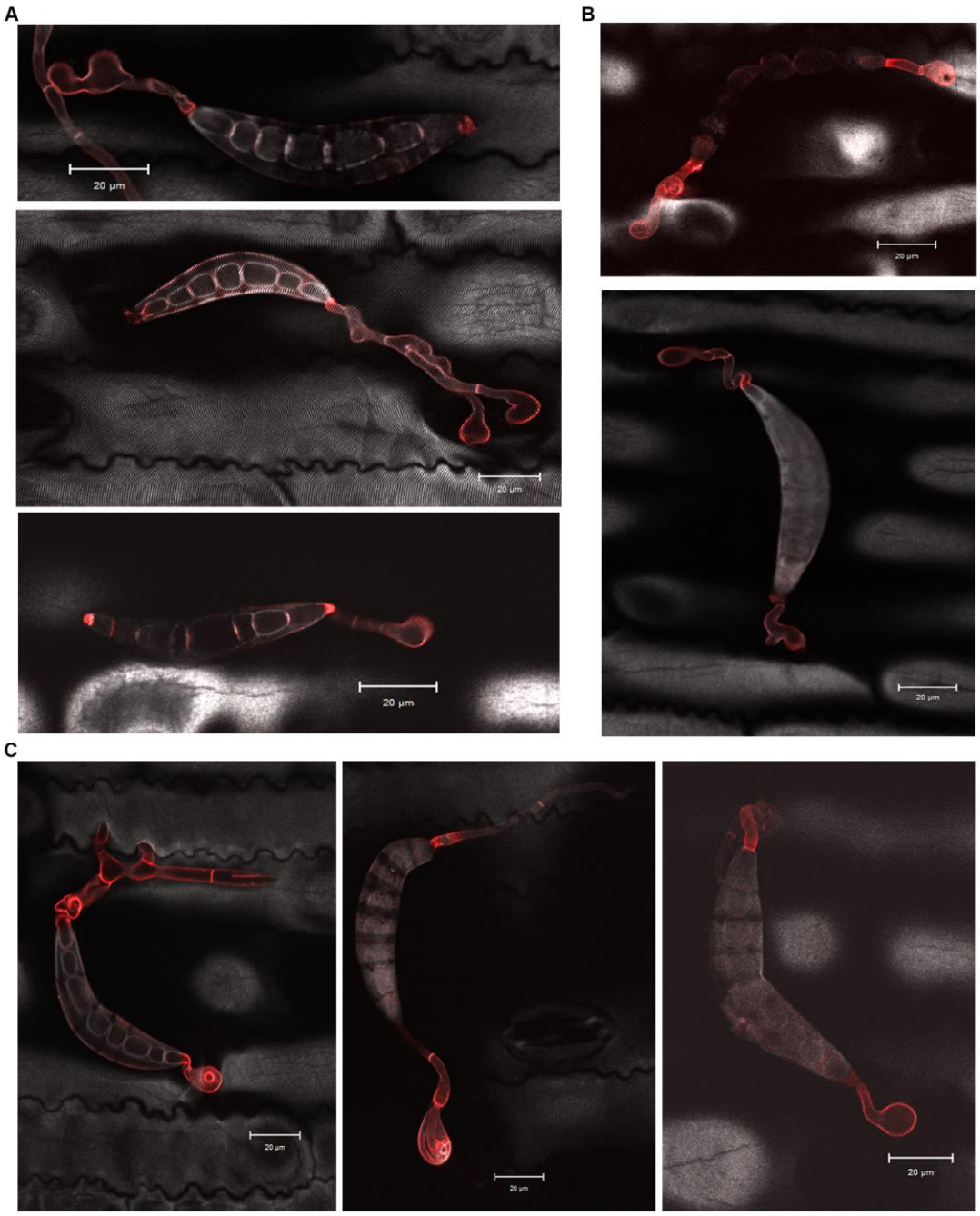

Figure 22 Germination**. A.** Spores showing growth from only one side of a spore. **B.** Spores that formed appressoria on both sides. **C.** Spores with only one appressorium.

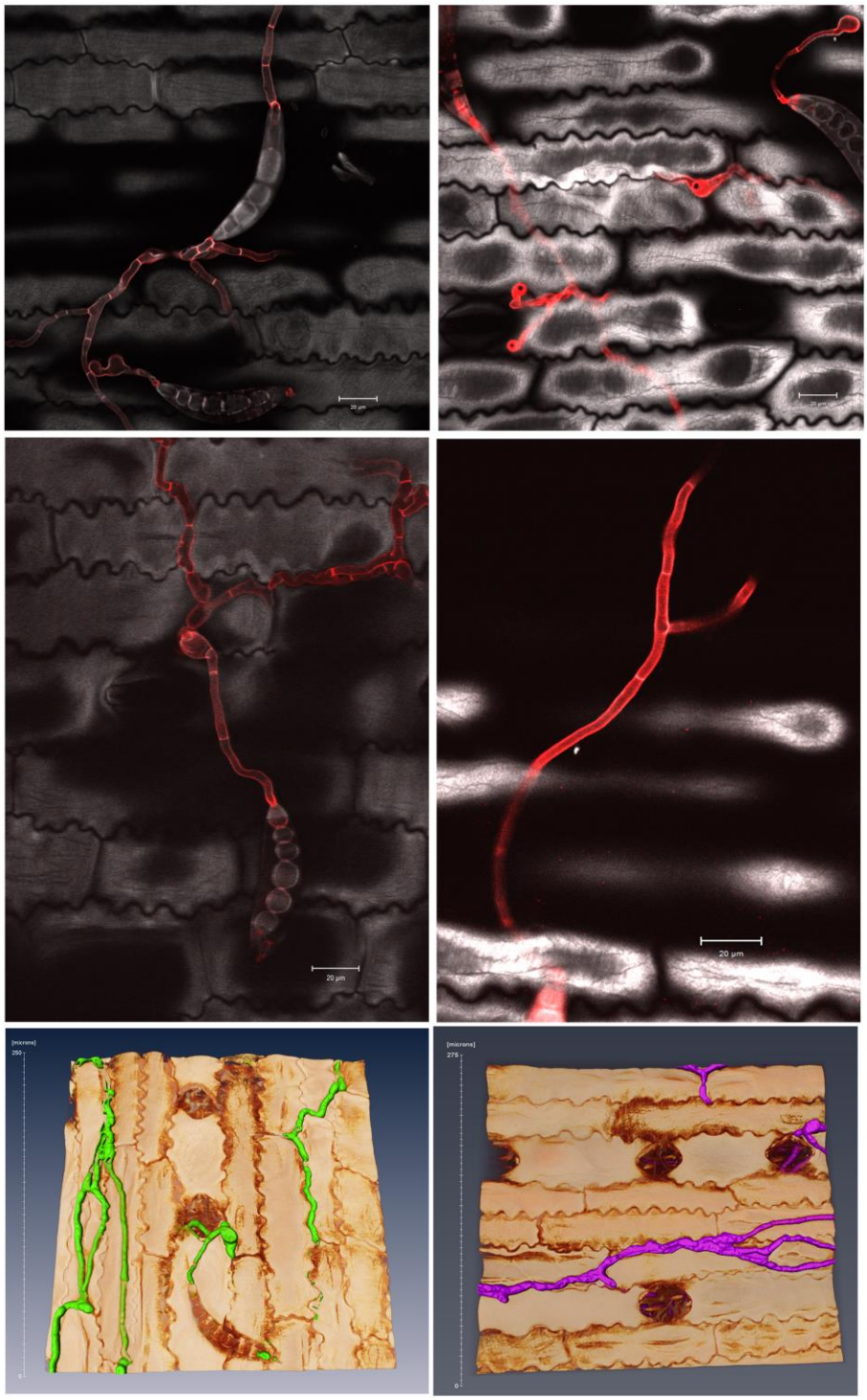

Figure 23 Surface growth

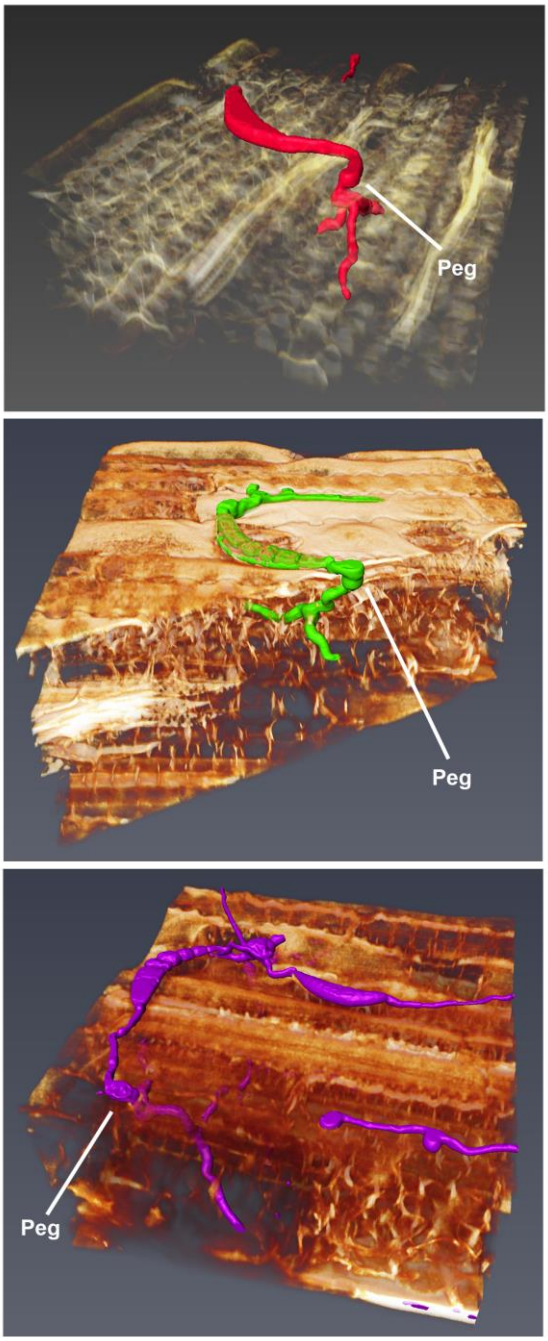

Figure 24 Penetration peg. 3D renderings all taken with a 40x magnification at a depth of approximately 350 microns. White arrows point to thinned out hyphae that appears to be a penetration peg.

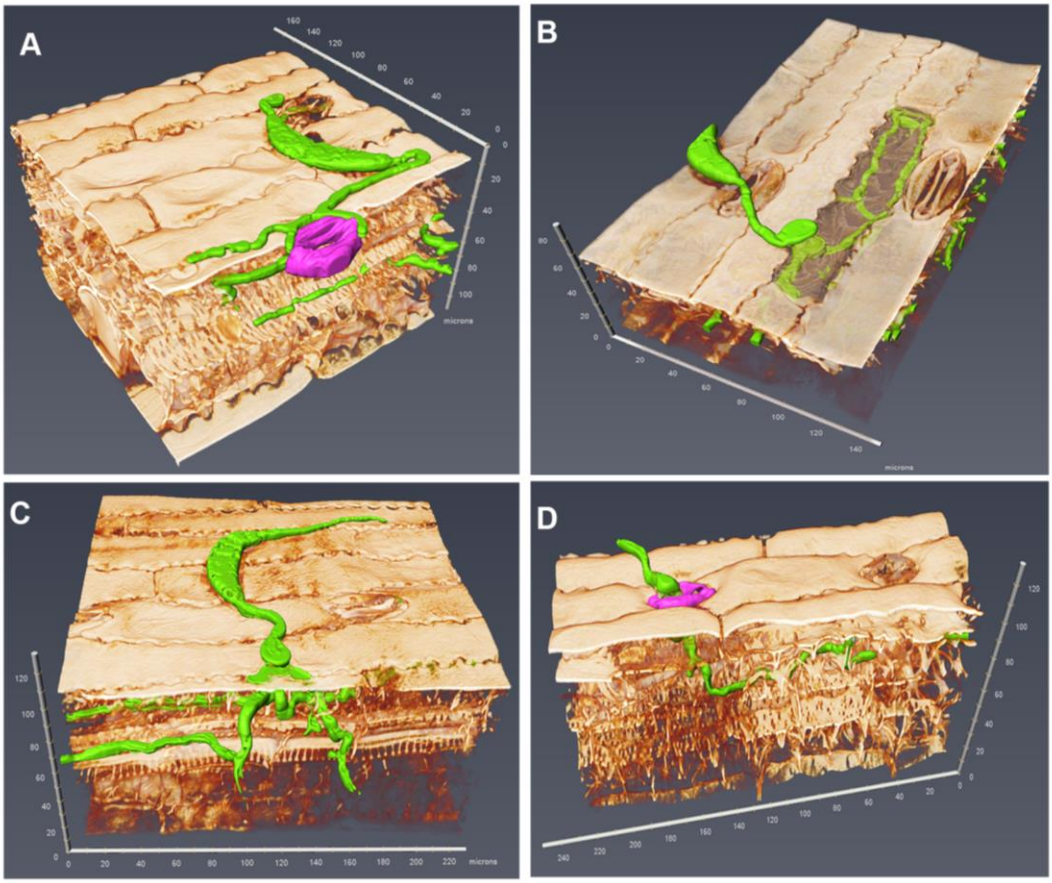

Figure 25 Penetration events. Fungus; green. Leaf; amber. **A.** Penetration occurring next to guard cell (pink). **B.** Intracellular penetration, infected epidermal cell segmented separately to enable transparency. **C.** Intercellular penetration. **D.** Penetration through guard cell (pink).

Hyphae formed branches in two ways; simple branches where one hyphal strand separates into two are frequently observed in surface growth and in open spaces of the mesophyll. Secondary branching, where the presence of a secondary structure that is essentially two or more branches radiating from a bulb of fungus, are seen most frequently following a penetration (Figure 26).

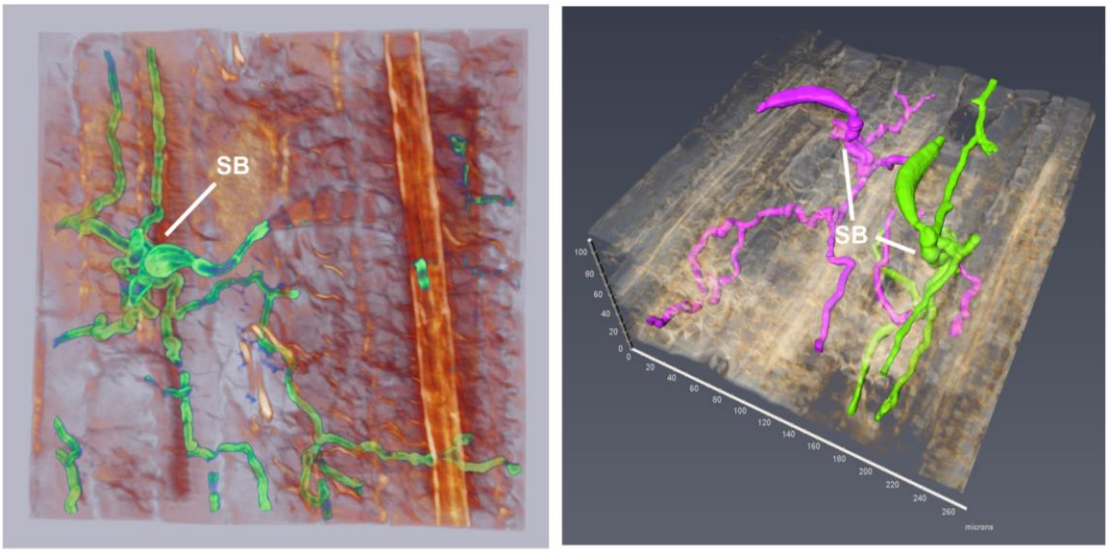

Figure 26 Secondary branching. Arrows point to a secondary branching structure.

Hyphae are seen extending loosely in open spaces in the mesophyll and twist in tight spaces between cells. Much of the distribution throughout the sample was seen localized near the vascular bundle (Figure 27). Shrouding around the vascular bundles is typical and should be expected considering their abundance of nutrients. The fungus is not reported to penetrate the vasculature but in at least one image, hyphae was seen inside the vasculature.

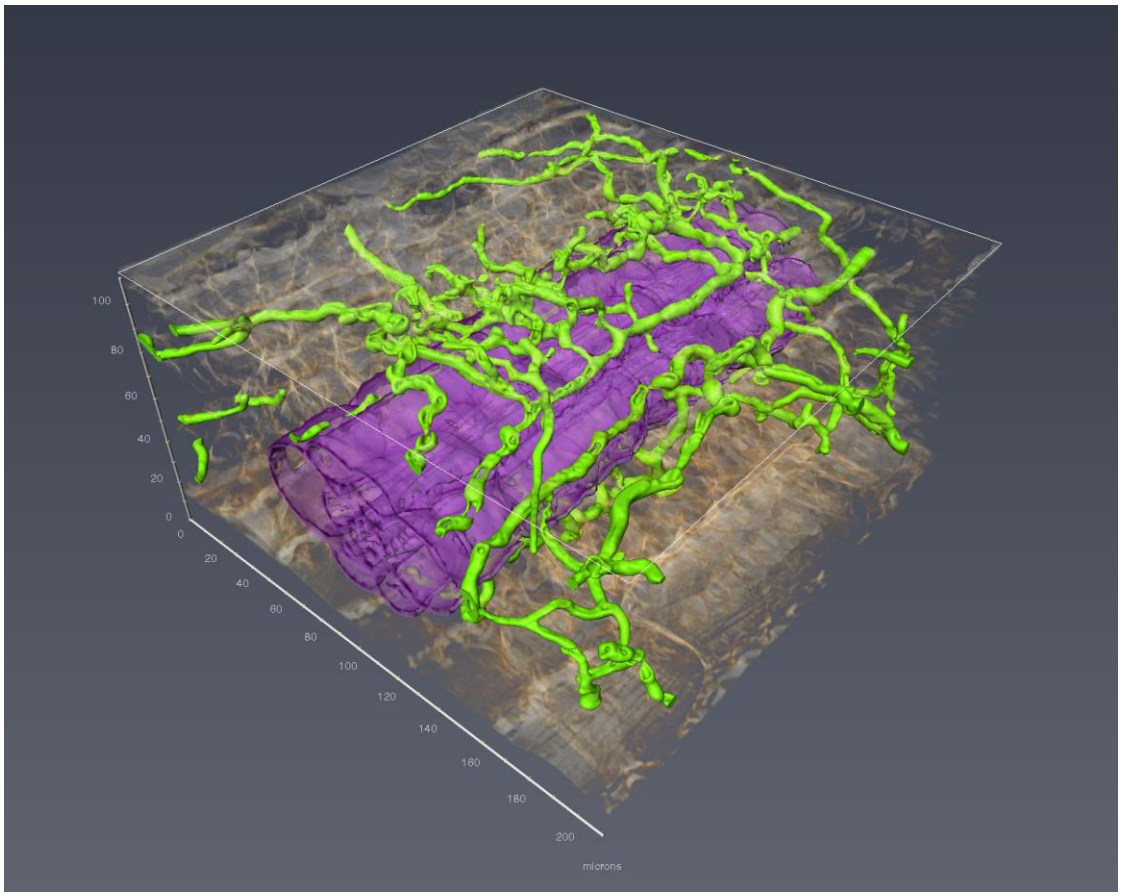

Figure 27 Distribution near vasculature**.** Hyphae (green) seen shrouding the vascular bundle (purple).

Chapter 4

DISCUSSION AND FUTURE DIRECTIONS

The investigation originally set forth attempted to quantify both *C.heterostrophous* and the related pathogen *Setosphaeria turcica.* However, the short duration of my time as a masters student narrowed my focus to an in depth study of *C.heterostrophous***.** I developed a technique for mounting and storing cleared samples that can be reimaged for several years. I also enhanced the clearing method by increasing the time required for KOH. I observed that samples mounted in glycerol experience a gradual loss in opacity compared with samples mounted in Sca*l*eP. Semi-automated, large scale fungal quantification methods established in this project, combined with high resolution investigation enabled the discovery of several interesting features of pathogenesis. When these methods are applied to NILs, many more cellular phenomena occurring at specific QTL.

A major advance of my research was determining the correct parameters required to image macroscopic samples (mm) at microscopic resolution (µm). For example, approximately one year of highspeed data collection at 10x was required to determine that we were oversampling in XY and undersampling in Z. We fixed this problem by increasing magnification and optimizing macro settings (Multitime) for 20x magnification that would maximize image information without compromising on time. There is a maximum number of tiles the macro is able to handle that put a limit on XY coverage. But, by using the same amount of tiles as with the 10x magnification, blank space was eliminated and data collection was maximized. Furthermore, the investment in a fast moving Piezo to quickly traverse through Z cut collection time in half.

The eventual goal of this project it to analyze numerous NIL pairs. Therefore, during my project I took steps to increase the speedand throughput of our assay. Since there are 12 samples for both lines at each time point, slides were first designed as 3x4 formation and 1200 tiles were collected over night for each slide. We are now mounting twice as many on a slide (4x6), which should double the data collection in an overnight setup. However, although Multitime could set and remember 2400 tile locations, errors often arose between 1600-2000 tiles stopping the image process entirely. These errors were likely related to a memory leak although it is still unclear what the issue is. Once the acquisition probem has been solved, my efforts developing a 24 sample mounting method will result in doubling our data collection rate.

The methods I developed have provided an unprecedented view of 3D fungal infection in maize, but improvements should be made to our protocol. For example, a better method for sealing should be identified. Previously, samples were sealed with VALAP, but that seal was easily broken. I used nail polish, which decreased the problem; however, the seal on some slides still broke and gradually lost fluid resulting in some samples drying out. It was also noticed that samples more than 2 years old have become thinner overtime which may result in inaccurate 3D data if too much time has elapsed. We are now investigating flexible silicone sealants that will be less likely to break, preserving the samples for long-term.

When this project was started tiling was preformed using the Fiji distribution of ImageJ. It was overwhelmingly time consuming and stitched images were inaccurate. When Abhishek Kolagunda joined as a computer science Ph.D. student, he modified the algorithm such that it preforms much faster and more precise stitching

for our samples. Tiling without shade corrections, left noticeable contrasting differences in each tile that resulted in dark, vertical stripes throughout the stitched image. To remove the shading artifact, I collected illumination profiles, which Abhishek used to create even intensity across each tile. Without this illumination adjustment, it would be impossible to accurately map the leaf surface for this data. Furthermore, some skeleton data and especially spore detection are effected by the uneven lighting therefore it is crucial that a corresponding profile image is captured with each overnight run.

Maximum intensity projections created from the highspeed tiled data enabled a great amount of hyphal quantification to be done. With Steve Rhein's contributions to measuring width, skeletonizing, and pruning, an enormous amount of data was generated. In Chapter 3 I presented the initial set of quantified characteristics extracted from the images was generated. We examined edge, node, and leaf features compared to hyphae length and saw interesting difference between Mo17 and B73 lines. Next, an analysis comparing the average widths of hyphae in each line at each time point may reveal some insights in fungal growth and pathogenesis. The work here is our first analysis of these data sets, but a large number of analytical possibilities for this data exist, and a multitude of biological interpretations can be drawn from it. This analysis was conducted in 2D maximum intensity projections; however algorithms to quantify highspeed data in 3D will help measure the difference in hyphae presence on the surface versus within the tissue and could possibly resolve hyphae within different tissue layers. Even more curious is the number of spores compared to hyphae growth. Using template matching and iterative learning algorithms, we are developing methods to detect spores and similarly shaped stomata.

Overall, more work on the algorithms that quantify the MIP of the fungal channel must be done before quantification can be done in 3D. Where it stands, the algorithm currently can gather basic information on the skeleton length, distribution of hyphal width, number of nodes, edges, and leaves. The best 3D data of course comes from multiphoton imaging. A protocol to automate the collection of multiphoton images should be established in the future so more events can be captures and rendered in 3D. Quantification of features like stomata and fungal spores are possible with the use of computer learning, however accurate data has yet to be gatheres for this set and this remains a work in progress.

There is a synergistic connection between the high throughput, large scale quantification and the high resolution, targeted studies on the multiphoton microscope. First, inferences made from quantitative data from the tiled images can be verified and then investigated further in high resolution multiphoton imaging. Second, analyzing pathogenesis in high resolution unraveled very exciting details about disease progression, which can then be used to guide future quantification of the tiled images. For example, we discovered that the fungus can infect between cells or directly into a cell. Intracellular penetration occurred frequently, which is not reported for this pathogen. More multiphoton images than expected showed hyphae that appeared trapped inside an epidermal cell it had penetrated. My discovery is now being used to guide the development of new algorithms to quantify types of penetration. They will be used to first look for differences between the parent Mo17 and B73 lines, and then eventually to analyse NILs.

Infection within the tissue was found predominately shrouding vascular bundles. Hyphae was seen growing parallel to the bundles and regularly in the grooves

of the xylem. The tissue samples that were investigated had mostly intermediate sized bundles that are associated with tightly packed sclerenchyma cells. Sclerenchyma cells contain a cell wall hardening component known as lignin and are specialized for support, they are dead at maturation. It was interesting to see how much infection took place in the tight spaces between these cells. One idea may be that because these cells are dead, the hyphae are safe from any potential defense mechanism provided by live cells. Harder, thicker cell walls may also increase the difficulties hyphae face as they attempt to penetrate and even extend throughout the tissue. We are now testing different stains for lignin see if this is truly a factor in resistance. In addition to lignin, there are numerous other fungal and plant characteristics that can be quantified.

A complete and exhaustive analysis on the characteristics and differences in B73 and Mo17 will provide a foundation on what to quantify in the NILs. Understanding the variances between these two completely different lines can help estimate the expected difference in closely related lines. Thoroughly documenting regular features of pathogenesis in high resolution well help distinguish an abnormal feature of pathogenesis that may result from a resistance mechanism. Our current method just looks at the cell walls that define the structure and physical interaction between the fungus and the host. To fully reach the potential of this approach, we will need to find ways to quantify more features such as lignin deposition, cuticle thickness, sugar distribution and potentially the cellular expression level of specific genes.

We have begun to collect data from a NIL. Samples for a B73-like NIL containing an introgression from chromosome bin 9.02 called P505 have been inoculated with *C.heterostrophous* and collected for imaging purposes. This particular

introgression is known to produce cafeoyl coA methyl transferase, an enzyme involved in a lignin production pathway. Inbred lines without this gene show far more susceptibility to the disease than when the gene is present. The exact disease phenotype of this particular gene is unclear. We expect that in future work the images of this P505 will show some difference in fungal presence compared with B73. More differences are expected to be observed in the high resolution investigation. I hypothesize that there will be increased lignin in P505 which will result in less intracellular penetration. Sclerenchyma cells in P505 may be thicker than those in B73, careful observations of hyphae in these areas should be made to better understand why pathogenesis is occurring there. It is possible that because of the added sclerenchyma cell wall strength provided by the lignin in P505, that less hyphae are even able to infect in the area around the vascular bundle, and even less hyphae are able to connect with each other, increasing disease resistance.

This project has laid the groundwork to produce previously unattainable amounts of microscopic data with macroscopic implications. Modifications in the clearing technique allowed for deeper optical clarity in leaf tissue samples which was necessary for mapping the top and bottom leaf surfaces. Techniques for mounting and storage of samples were improved upon greatly and enabled the preservation and reimaging of samples for multiple years. The highspeed confocal microscope, coupled with a fast moving Piezo allowed for me to capture a large amount of image data with 20x magnification without compromising on time. This, along with enhancements in stitching speed and a user friendly macro was essential in establishing the semi-automated pipeline to generate image data and quantitative analysis of fungal networks. Other researchers can apply these imaging techniques to any number of

projects, but it would be most exciting to see this design carried out to elucidate other QTL in maize.

REFERENCES

1. Crop Water Information: Maize. *Food and Agriculture Organization of the United Nations* at <http://www.fao.org/nr/water/cropinfo_maize.html>

2. Kump, K. L. *et al.* Genome-wide association study of quantitative resistance to southern leaf blight in the maize nested association mapping population. *Nat. Genet.* **43,** 163–8 (2011).

3. Poland, J. a, Balint-Kurti, P. J., Wisser, R. J., Pratt, R. C. & Nelson, R. J. Shades of gray: the world of quantitative disease resistance. *Trends Plant Sci.* **14,** 21–9 (2009).

4. Vale, F. X. R. Do, Parlevliet, J. E. & Zambolim, L. Concepts in plant disease resistance. *Fitopatol. Bras.* **26,** 577–589 (2001).

5. Ayliffe, M. *et al.* A simple method for comparing fungal biomass in infected plant tissues. *Mol. Plant. Microbe. Interact.* **26,** 658–67 (2013).

6. Minker Katharine R., Meredith L. Biedrzycki, Abhisek Kolagunda, Stephen Rhein, Fabiano J. Perina, Samuel S. Jacobs, Michael Moore, Tiffany M. Jamann, Rebecca Nelson, Qin Yang, Peter Balint-Kurti, Chandra Kambhamettu, Randall J. Wisser, J. L. C. *Semi-automated confocal imaging of fungal pathogenesis on plants: microscopic analysis of macroscopic specimens.* (2015).

7. Russell, S. H. & Evert, R. F. Leaf vasculature in Zea mays L. *Planta* **164,** 448–458 (1985).

8. Schnable, P. S. *et al.* The B73 Maize Genome: Complexity, Diversity, and Dynamics. *Science (80-.).* **326,** 1112–1115 (2009).

9. Chandler, V. L. & Brendel, V. The Maize Genome Sequencing Project\n(Update on the Maize Genome Sequencing Project). *Plant Physiol.* **130,** 1594–1597 (2002).

10. Liu, K. *et al.* Genetic Structure and Diversity among Maize Inbred Lines as Inferred from DNA Microsatellites. *Genetics* **165,** 2117–2128 (2003).

11. Yu, J., Holland, J. B., McMullen, M. D. & Buckler, E. S. Genetic Design and Statistical Power of Nested Association Mapping in Maize. *Genetics* **178,** 539–551 (2008).

12. Wisser, R. J., Sun, Q., Hulbert, S. H., Kresovich, S. & Nelson, R. J. Identification and characterization of regions of the rice genome associated with broad-spectrum, quantitative disease resistance. *Genetics* **169,** 2277–2293 (2005).

13. Kump, K. L., Holland, J. B., Jung, M. T., Wolters, P. & Balint-Kurti, P. J. Joint

Analysis of Near-Isogenic and Recombinant Inbred Line Populations Yields Precise Positional Estimates for Quantitative Trait Loci. *Plant Genome J.* **3,** 142 (2010).

14. Eichten, S. R. *et al.* B73-Mo17 Near-Isogenic Lines Demonstrate Dispersed Structural Variation in Maize. *Plant Physiol.* **156,** 1679–1690 (2011).

15. Condon, B. J. *et al.* Comparative Genome Structure, Secondary Metabolite, and Effector Coding Capacity across Cochliobolus Pathogens. *PLoS Genet.* **9,** e1003233 (2013).

16. Ohm, R. A. *et al.* Diverse lifestyles and strategies of plant pathogenesis encoded in the genomes of eighteen Dothideomycetes fungi. *PLoS Pathog.* **8,** e1003037 (2012).

17. Yoder, O. c. in *Genetics of Plant Pathogenic Fungi Volume 6* 93–111 (1988).

18. Wheeler, H. Ultrastructure of penetration by Helminthosporium maydis. *Physiol. Plant Pathol.* **11,** 171–178 (1977).

19. Sørensen, C. K., Justesen, A. F. & Hovmøller, M. S. 3-D imaging of temporal and spatial development of Puccinia striiformis haustoria in wheat. *Mycologia* **104,** 1381–9 (2012).

20. Buda, G. J., Isaacson, T., Matas, A. J., Paolillo, D. J. & Rose, J. K. C. Three-dimensional imaging of plant cuticle architecture using confocal scanning laser microscopy. *Plant J.* **60,** 378–85 (2009).

21. Lichtman, J. W. & Conchello, J.-A. Fluorescence microscopy. *Nat. Methods* **2,** 910–919 (2005).

22. Minsky, M. Microscopy apparatus. (1961).

23. Földes-Papp, Z., Demel, U. & Tilz, G. P. Laser scanning confocal fluorescence microscopy: An overview. *Int. Immunopharmacol.* **3,** 1715–1729 (2003).

24. Im, K.-B., Han, S., Park, H., Kim, D. & Kim, B.-M. Simple high-speed confocal line-scanning microscope. *Opt. Express* **13,** 5151 (2005).

25. Dunn, K.W. Young, P. A. Principles of Multiphotn Microscopy. *Nephron Exp. Nephrol.* **103,** 33–40 (2006).

26. Wuyts, N. *et al.* Open Access High-contrast three-dimensional imaging of the Arabidopsis leaf enables the analysis of cell dimensions in the epidermis and mesophyll. 1–14 (2010).

27. Warner, C. a *et al.* An optical clearing technique for plant tissues allowing deep imaging and compatible with fluorescence microscopy. *Plant Physiol.* **166,** 1684–7 (2014).

28. Palmer, W. M. *et al.* PEA-CLARITY: 3D molecular imaging of whole plant organs. *Nat. Publ. Gr.* 1–6 (2015). doi:10.1038/srep13492

29. Obrien, P. Autoclaving as an aid in the clearing of plant specimens. **40,** 40–41 (1974).

30. Talbot, M. J. & White, R. G. Cell surface and cell outline imaging in plant tissues using the backscattered electron detector in a variable pressure scanning electron microscope. *Plant Methods* **9,** 40 (2013).

31. Villani, T. S., Koroch, A. R. & Simon, J. E. An Improved Clearing and Mounting Solution to Replace Chloral Hydrate in Microscopic Applications. *Appl. Plant Sci.* **1,** 1300016 (2013).

32. Rath, M., Grolig, F., Haueisen, J. & Imhof, S. Combining microtomy and confocal laser scanning microscopy for structural analyses of plant-fungus associations. *Mycorrhiza* 1–8 (2013). doi:10.1007/s00572-013-0530-y

33. Chung, C.-L. *et al.* Resistance loci affecting distinct stages of fungal pathogenesis: use of introgression lines for QTL mapping and characterization in the maize--Setosphaeria turcica pathosystem. *BMC Plant Biol.* **10,** 103 (2010).

34. Hama, H. *et al.* Scale: a chemical approach for fluorescence imaging and reconstruction of transparent mouse brain. *Nat. Neurosci.* **14,** 1481–8 (2011).

35. Monsigny, M., Roche, a C., Sene, C., Maget-Dana, R. & Delmotte, F. Sugar-lectin interactions: how does wheat-germ agglutinin bind sialoglycoconjugates? *Eur. J. Biochem.* **104,** 147–153 (1980).

36. Schindelin, J. *et al.* Fiji: an open-source platform for biological-image analysis. *Nat. Methods* **9,** 676–82 (2012).

37. Preibisch, S., Saalfeld, S. & Tomancak, P. Globally optimal stitching of tiled 3D microscopic image acquisitions. *Bioinformatics* **25,** 1463–5 (2009).